

Origin of minimal conductivity in Dirac materials: Momentum-dependent self-energy function from long-ranged disorder scattering

Weiwei Chen¹, Yedi Shen,² Bo Fu^{3,4}, Qinwei Shi,² and W. Zhu^{5,*}


¹Key Laboratory of Intelligent Manufacturing Quality Big Data Tracing and Analysis of Zhejiang Province, College of Science, China Jiliang University, Hangzhou 310018, China

²Hefei National Laboratory for Physical Sciences at the Microscale, and Synergetic Innovation Center of Quantum Information and Quantum Physics, University of Science and Technology of China, Hefei, Anhui 230026, China

³School of Sciences, Great Bay University, Dongguan 523000, Guangdong Province, China

⁴Department of Physics, The University of Hong Kong, Pokfulam Road, Hong Kong, China

⁵School of Science, Westlake University, Hangzhou 310024, China

 (Received 18 November 2022; revised 14 November 2023; accepted 15 November 2023; published 29 November 2023)

We present a unified understanding of the experimentally observed minimal dc conductivity in Dirac materials. First, based on the linear response theory, we reveal that the momentum-dependent self-energy function induces a tunable minimal conductivity in Dirac electrons, the magnitude of which is directly related to the coefficient of the momentum-dependent part in the self-energy function. Taking the long-ranged Gaussian and Coulomb potentials as examples, the momentum-dependent self-energy function is perturbatively derived using the Born approximation and supplemented by the self-consistent Born approximation and renormalization group analysis. Moreover, we further validate our theory via numerical simulations using the large-scale Lanczos algorithm. The explicit momentum dependence of the self-energy on the intensity, concentration, and range of potential are critically addressed. Therefore, our theory provides a reasonable interpretation of the sample-dependent minimal conductivity observed in experiments.

DOI: [10.1103/PhysRevB.108.174205](https://doi.org/10.1103/PhysRevB.108.174205)

I. INTRODUCTION

In the past decades, a large class of materials that possess linear energy dispersion described by the effective Dirac-like electrons has been discovered, of which monolayer graphene is a representative example. The earliest experimental measurements on graphene reported a finite dc conductivity $\sigma_{\min} \approx \frac{4e^2}{h}$ at the Dirac point at low temperature [1,2], dubbed the minimal conductivity. The observed value is larger than the earlier prediction of $\sigma_{\min} = \frac{4e^2}{\pi h}$ [3–6], giving rise to the famous “missing π ” problem [7]. To address this problem, subsequent experiments have been carried out [8–17], which show that the minimal conductivity is strongly sample dependent, i.e., $\sigma_{\min} = C \frac{4e^2}{\pi h}$, with the factor C varying from 1.7 to 10, indicating the crucial role of randomness or disorder in these Dirac materials.

The transport properties of two-dimensional disordered Dirac fermions have been intensively studied for the d -wave superconductivity in the cuprate superconductors [5,6] and the plateau transition in the integer quantum Hall effect [3]. The discovery of graphene rejuvenated this problem. The previous theoretical results for σ_{\min} can be mainly summarized as (i) a scattering-independent value $\sigma_{\min} = \frac{4e^2}{\pi h}$ [3–6,18–22], which is independent of the strength and nature of the disorder; (ii) a universal value $\sigma_{\min} \approx \frac{4e^2}{h}$, which is due to the quantum criticality of graphene in the vicinity of the Dirac point [23–25];

(iii) a universal value $\sigma_{\min} = \frac{\pi e^2}{2h}$ [26,27], from the ac Kubo formula, derived by removing the smearing of the single-particle Green’s functions before taking the dc limit; (iv) a disorder-dependent σ_{\min} [28–34]. In particular, although some previous studies have yielded a disorder-dependent minimal conductivity, most of these are based on semiclassical Boltzmann transport theory [28–31], ignoring the disorder induced quantum corrections near the Dirac point. Since Boltzmann theory is not applicable around the Dirac point [7], a fully quantum mechanical treatment is highly desirable in order to address the minimal conductivity.

In parallel, numerical calculations have also addressed this problem using various approaches [32,35–38]. Noro *et al.* find that the minimal conductivity at the Dirac point remains universal in the clean limit, but increases with disorder and becomes nonuniversal for long-range scatterers, by numerically solving the self-energy and current vertex function [35]. Nomura and MacDonald numerically calculated σ_{\min} using the Kubo formula and found that σ_{\min} is a few times larger for long-ranged Coulomb scatterers than for short-range scatterers [36]. Similar results were also obtained by numerically calculating the transmission matrix [37]. In addition, Lima and Lewenkopf numerically studied the effect of charge puddles, which are generated by a long-range local potential, on the conductivity minimum of graphene, and also concluded that the transmission is enhanced at the charge neutrality point [38]; however, a full analytical understanding beyond the numerical calculation is still lacking. These numerical results, which are beyond the aforementioned theoretical descriptions,

*zhuwei@westlake.edu.cn

TABLE I. Dimensionless parameter α for different types of disorder potentials. \mathbf{R}_i and N_{imp} are the location and total number of impurities, ξ is the characteristic length scale of Gaussian potential, the strength $\pm u_0$ is randomly distributed with equal probability, κ is the static dielectric constant, A_c is the area of the primitive cell, q_s is the Thomas-Fermi screening constant, k_c is the ultraviolet momentum cutoff, and n_i is the concentration of the impurities.

| Potential | Length scale | α |
|--------------------|---------------|---|
| Gaussian [Eq. (3)] | $\xi \ll a$ | $\frac{n_i u_0^2}{2(\hbar v_f)^2} \frac{A_c k_c^2 \xi^2}{8\pi}$ [Eqs. (7) and (25)] |
| | $\xi \gg a$ | $\frac{n_i u_0^2}{2(\hbar v_f)^2} \frac{\pi \xi^4}{A_c}$ [Eqs. (7) and (25)] |
| Coulomb [Eq. (8)] | $1/q_s \ll a$ | $(\frac{e^2}{\kappa})^2 \frac{2\pi n_i k_c^2}{(\hbar v_f)^2 q_s^4}$ [Eqs. (9) and (30)] |
| | $1/q_s \gg a$ | $(\frac{e^2}{\kappa})^2 \frac{2\pi n_i}{(\hbar v_f)^2 q_s^3}$ [Eqs. (9) and (30)] |

urgently call for a reasonable analytical interpretation of the minimal conductivity.

In this paper, we offer a general picture for understanding the sample-dependent minimal conductivity in Dirac materials by studying the effect of long-ranged random potentials. The long-ranged randomness could be realized by screened charges in the substrate [37–40], local strain fluctuations [16,17], and other defects that vary smoothly on the atomic scale [9,30]. In the presence of long-ranged random potentials, we elucidate that the self-energy is momentum dependent, which is overlooked in most of the existing literature. Moreover, in some works that considered the momentum dependence of the self-energy, its effect is also eliminated due to the simultaneously applied on-shell approximation [28–31]. Crucially, the electric minimal conductivity, evaluated via the standard Kubo formula under disorder configuration average by taking into account the corrected self-energy, obeys the relationship $\sigma_{\text{min}} = \frac{1}{(1-\alpha)^2} \frac{4e^2}{\pi h}$ [Eq. (19)], where the leading momentum-dependent correction is parametrized by a dimensionless parameter α , the expressions of which for different types of disorder potentials are shown in Table I. This finding, in sharp contrast to the disorder-independent values in previous studies [3–6,18–27], provides a simple and physically appealing explanation for the observed minimum conductivity in experiments.

The paper is organized as follows. In Sec. II, we present the basis of our investigated model, including the Hamiltonian, velocity, Green's function, and disorder potentials we considered. Our main result is shown in Sec. III where the minimal conductivity is calculated by the Kubo formula with an assumed momentum-dependent self-energy function. Then, the self-energy functions in the long-ranged disorder potentials are derived and analyzed based on the Born approximation in Sec. IV A, SCBA in Sec. IV B, renormalization group in Sec. IV C, and numerical simulation in Sec. IV D. Finally, the conclusion and discussion are summarized in Sec. V. Various details of the analytical derivation are presented in the Appendixes.

II. MODEL

The charge carriers of graphene near half filling can be modeled by a Dirac Hamiltonian

$$H = \hbar v_f \boldsymbol{\sigma} \cdot \mathbf{k} + U(\mathbf{r}), \quad (1)$$

where $v_f \approx 10^6 \text{ m s}^{-1}$ is the Fermi velocity, $\boldsymbol{\sigma} = (\sigma_x, \sigma_y)$ are the Pauli matrices of pseudospin (sublattice), $\mathbf{k} = (k_x, k_y)$ is a two-component wave vector, and $U(\mathbf{r})$ describes the long-ranged random potential that is experienced by the Dirac electrons. For simplicity, we model $U(\mathbf{r})$ by several typical forms (see Table I). We ensure that the results shown below are not sensitive to the form of the potentials. In the disorder-free case, the eigenvalue and eigenfunction of the Hamiltonian Eq. (1) are

$$E_{ks} = s \hbar v_f k, \quad \Psi_{ks}(\mathbf{r}) = \frac{e^{i\mathbf{k} \cdot \mathbf{r}}}{\sqrt{2\mathcal{V}}} \begin{pmatrix} 1 \\ s e^{i\theta_{\mathbf{k}}} \end{pmatrix}, \quad (2)$$

where $s = \pm$ denotes the band index, \mathcal{V} is the sample area, and $\theta_{\mathbf{k}} = \arctan(k_y/k_x)$. Based on the eigenfunction, the matrix $U_{\mathbf{k}}$ which implements the rotation from pseudospin to eigenstates basis has the form

$$U_{\mathbf{k}} = \frac{1}{\sqrt{2}} \begin{pmatrix} 1 & 1 \\ e^{i\theta_{\mathbf{k}}} & -e^{i\theta_{\mathbf{k}}} \end{pmatrix}. \quad (3)$$

Therefore, the velocity operator along the x direction in the eigenstates basis is

$$v_x(\mathbf{k}) = U_{\mathbf{k}}^\dagger \frac{\partial H}{\partial \hbar k_x} U_{\mathbf{k}} = v_f (\cos \theta_{\mathbf{k}} \sigma_z + \sin \theta_{\mathbf{k}} \sigma_y). \quad (4)$$

In this work, we consider two typical long-ranged disorders: long-ranged Gaussian and Coulomb potential. The long-ranged Gaussian potential in graphene lattice is expressed as

$$U(\mathbf{r}) = \sum_{i=1}^{N_{\text{imp}}} \pm u_0 e^{-\frac{|\mathbf{r}-\mathbf{R}_i|^2}{\xi^2}}, \quad (5)$$

where ξ is the characteristic length scale, N_{imp} is the number of impurity, and impurities of $\pm u_0$ are randomly distributed with equal probability. The correlation function of the long-ranged Gaussian potential in the momentum space is

$$\mathcal{K}_G(\mathbf{q}) = \langle U(\mathbf{q})U(-\mathbf{q}) \rangle = K_0 (\hbar v_f)^2 e^{-\frac{\xi^2 q^2}{2}}, \quad (6)$$

where K_0 is a dimensionless parameter parametrizing the magnitude of the potential, which has different expressions for sharp ($\xi \ll a$) and smooth ($\xi \gg a$) potentials [37,39]

$$K_0 = \frac{n_i u_0^2}{(\hbar v_f)^2} \begin{cases} \frac{A_c}{2}, & \xi \ll a, \\ \frac{2\pi^2}{A_c} \xi^4, & \xi \gg a, \end{cases} \quad (7)$$

where $a = 1.42 \text{ \AA}$ is the carbon-carbon distance of graphene, $A_c = \frac{3}{2} a^2$ is the area of the primitive cell, and $n_i = N_{\text{imp}}/N$ is the impurity concentration.

Another disorder we considered, long-range screened Coulomb potential, has the form in real space as

$$V(\mathbf{r}) = \pm \frac{e^2}{\kappa r} e^{-q_s r}, \quad (8)$$

where κ is the static dielectric constant, scatters of \pm are randomly distributed with equal probability, and q_s is the Thomas-Fermi screening constant. The correlation function of long-range screened Coulomb potential in momentum space

is

$$\mathcal{K}_C(\mathbf{q}) = \langle V(\mathbf{q})V(-\mathbf{q}) \rangle = \frac{n_i V_0^2}{q_s^2 + q^2}, \quad \text{with } V_0 = \frac{2\pi e^2}{\kappa}, \quad (9)$$

where n_i are the concentration of impurities.

The Green's function of the disordered system in the eigenstate basis is given by

$$G^{R/A}(\mathbf{k}, E) = \begin{pmatrix} g_+^{R/A}(\mathbf{k}, E) & 0 \\ 0 & g_-^{R/A}(\mathbf{k}, E) \end{pmatrix}, \quad (10)$$

with

$$g_s^{R/A}(\mathbf{k}, E) = \frac{1}{E - E_{k,s} - \Sigma(\mathbf{k}, E)}, \quad (11)$$

where $\Sigma(\mathbf{k}, E)$ is the self-energy induced by disorder potential.

III. MINIMAL CONDUCTIVITY WITH MOMENTUM-DEPENDENT SELF-ENERGY

In general, the electron self-energy induced by the impurity scattering is both momentum and energy dependent. For the short-ranged disorder potential, the momentum dependence of the self-energy is negligible since the potential can be Fourier transformed into the sum of equal-weighted plane waves in the momentum space. The long-range disorder potential, the Fourier transformation of which is the sum of momentum-dependent weighted plane waves, naturally causes momentum-dependent scattering. However, the momentum dependence in the long-ranged disorder-induced self-energy function has also been neglected in most of the previous works. One commonly used treatment is the on-shell approximation ($E = E_{k,s}$) [28–31], i.e., the momentum and energy dependence of the self-energy is coupled by the dispersion relation in the clean limit. Moreover, the Feynman diagram of the self-energy function is simplified by assuming independence on the external momenta [19,41]. One of the motivations for this paper is to elucidate that this on-shell approximation is not well justified around the Dirac point, leading to a decoupled momentum-dependent self-energy function. The main result of this work is that we reveal the influence of such a momentum-dependent self-energy function on the minimal conductivity.

Before performing the analytical derivation and numerical calculation of the self-energy function for specific types of disorder, we assume that the self-energy function contains a nonzero momentum-dependent contribution,

$$\Sigma(\mathbf{k}s, E) \approx \Sigma_1(E) - \alpha s \hbar v_f k + i \Sigma_2(E), \quad (12)$$

where $\Sigma_1(E)$ and $\Sigma_2(E)$ describe the real and imaginary parts of the energy-dependent terms. Since the long-ranged random scalar disorder we considered here does not on average break the particle-hole symmetry [42–44], the self-energy in the eigenstate basis satisfies the relations $\text{Re}\Sigma(\mathbf{k}+, E) = -\text{Re}\Sigma(\mathbf{k}-, -E)$ and $\text{Im}\Sigma(\mathbf{k}+, E) = \text{Im}\Sigma(\mathbf{k}-, -E)$, which preserves the dispersion relation and broadens the width of the conduction and valence bands symmetrically about the Dirac point [45]. Then, we study the influence of this momentum-dependent self-energy function Eq. (12) on the minimal conductivity.

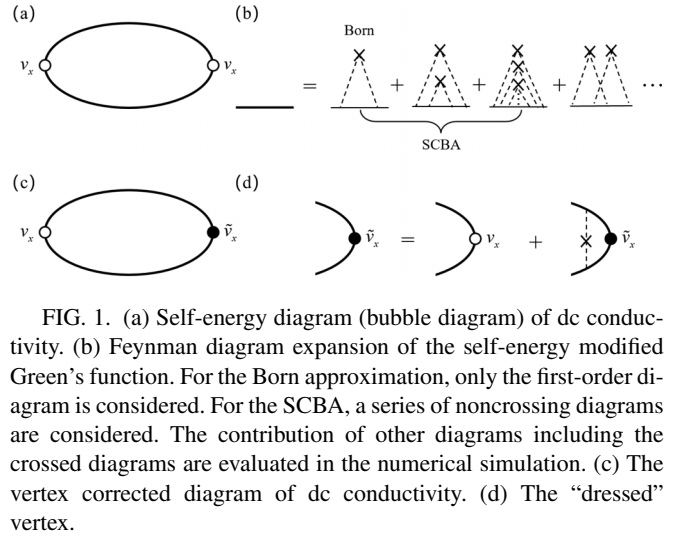


FIG. 1. (a) Self-energy diagram (bubble diagram) of dc conductivity. (b) Feynman diagram expansion of the self-energy modified Green's function. For the Born approximation, only the first-order diagram is considered. For the SCBA, a series of noncrossing diagrams are considered. The contribution of other diagrams including the crossed diagrams are evaluated in the numerical simulation. (c) The vertex corrected diagram of dc conductivity. (d) The “dressed” vertex.

Based on linear response theory, we can calculate the longitudinal conductivity at zero temperature using the Kubo formula [46]

$$\sigma_{xx}(E) = \sigma_{xx}^{RA}(E) - \text{Re}[\sigma_{xx}^{RR}(E)], \quad (13)$$

with

$$\sigma_{xx}^{RA}(E) = 4 \frac{e^2 \hbar}{2\pi \mathcal{V}} \text{Tr}[G^R(E)v_x G^A(E)v_x]_c, \quad (14)$$

$$\sigma_{xx}^{RR}(E) = 4 \frac{e^2 \hbar}{2\pi \mathcal{V}} \text{Tr}[G^R(E)v_x G^R(E)v_x]_c, \quad (15)$$

where the factor 4 denotes the degeneracy of the real spin and valley, Tr means the trace over both wave vector and pseudospin (sublattice) spaces, and the subscript c indicates a disorder configuration average. Here the RA contribution is analogous to the transport of classical particles within the relaxation time approximation and gives results close to conventional Boltzmann theory, while the RR contribution comes from calculations with a fully quantum mechanism and can be ignored in the limit $E\tau \gg 1$ (but not when $E\tau \ll 1$).

Using the assumed momentum-dependent self-energy function Eq. (12), we can write the Green's function for quasiparticle as

$$g_s^{R/A}(\mathbf{k}, E) = \frac{1}{a - (1 - \alpha)s \hbar v_f k + i \eta}, \quad (16)$$

where

$$\begin{aligned} a &= E - \Sigma_1(E), \\ \eta &= -\Sigma_2(E). \end{aligned} \quad (17)$$

Plugging the velocity Eq. (4), Green's function Eq. (10), and Eq. (16) into the Kubo formula Eq. (13), the leading order of the conductivity contributed from the bubble diagram, as shown in Fig. 1(a), is given by (details in Appendix A)

$$\begin{aligned} \sigma_{xx}(E) &= \frac{2e^2}{\pi h} \frac{1}{(1 - \alpha)^2} \left(1 + \frac{a}{\eta} \arctan \frac{a}{\eta} \right) \\ &\quad + \frac{2e^2}{\pi h} \frac{1}{(1 - \alpha)^2} \frac{\eta}{a} \arctan \frac{a}{\eta}, \end{aligned} \quad (18)$$

where the first and second terms denote the electron-hole incoherent (related to the terms $g_{+}^R g_{+}^A$, $g_{+}^R g_{+}^R$, $g_{-}^R g_{-}^A$, and $g_{-}^R g_{-}^R$) and coherent (related to the terms $g_{+}^R g_{-}^A$, $g_{-}^R g_{+}^A$, and $g_{-}^R g_{+}^R$) contributions, respectively. Therefore, the corresponding minimal conductivity at the Dirac point ($E = 0$) is

$$\sigma_{\min} = \frac{1}{(1-\alpha)^2} \frac{4e^2}{\pi h}. \quad (19)$$

Here we would like to give some remarks. First, Eq. (19) is similar to some other previous calculations based on the Kubo formula [18,19], including electron-hole coherent and incoherent contributions in RA and RR terms, which is beyond traditional Boltzmann transport theory where the electron-hole incoherent and retarded-retarded (RR) channel contribution are usually discarded or not completely considered. Second, the Ward's identity is not satisfied in the above calculation, since we have calculated the self-energy correction in the single-particle Green's function, but did not include the corresponding correction in the vertex. Thus we also estimate the vertex correction of the Kubo formula, which corresponds to the ladder Feynman diagrams shown in Figs. 1(c) and 1(d), using the long-ranged Gaussian potential (details in Appendix B). The vertex corrected minimal conductivity is

$$\sigma_{\min}^v = \frac{4e^2}{\pi h} \frac{1}{(1-\alpha)^2} \frac{1}{1 - \left[\frac{K_0}{4\pi(1-\alpha)^2} \right]^2}. \quad (20)$$

Since typical experiment conditions of high mobility graphene correspond to $K_0 \lesssim 1$, the influence of vertex correction to the minimal conductivity is much smaller than those induced by the linear momentum dependent self-energy in the bubble diagram. This is consistent with previous works showing that the vertex correction is negligible for calculations of the minimal conductivity [4,6]. In addition to the bubble and ladder Feynman diagrams, the Cooperon diagram associated with the weak and antiweak localization also contributes to the minimal conductivity [33,34] but, in this work, we provide an explanation for sample-dependent minimal conductivity from the diffusive mode, so we do not consider it. Third, σ_{\min} is significantly influenced by the momentum-dependent term ($\alpha \hbar v_f k$) of the self-energy, but independent of the energy-dependent part [$\Sigma_1(E)$ and $\Sigma_2(E)$], which explains why the majority of previous theoretical studies predicted $\sigma_{\min} = \frac{4e^2}{\pi h}$, independent of the strength and nature of the disorder [3–6,18–22]. Fourth, for long range disorder, the momentum contribution to the self-energy function has been reported; however, the role of it on the transport was unfortunately washed out in the widely used on-shell approximation [28–31]. Therefore, we claim that the application of the on-shell approximation around the Dirac point is questionable. Finally, with all of these nontrivial improvements, we point out that Eq. (19) shows that the minimal conductivity is enhanced by disorder. One interpretation is that the presence

of potential fluctuations smooth on the scale of the graphene lattice spacing increases the conductivity through quantum interference effects [31,32,35–37].

IV. SELF-ENERGY FUNCTION

In the previous section, we have shown that the minimal conductivity is deeply related to the momentum-dependent term in the self-energy function. In the following, we calculate the self-energy function analytically and numerically in the cases of the long-ranged Gaussian and Coulomb potential, from which the explicit momentum dependence of the self-energy on the intensity, concentration, and range of potential are critically addressed.

A. Born approximation

1. Long-ranged Gaussian potential

At first, we consider the long-ranged Gaussian potential based on the Born approximation; the corresponding self-energy is given by

$$\Sigma^B(\mathbf{k}s, E) = \frac{1}{V} \sum_{\mathbf{k}', s'} \mathcal{K}_G(\mathbf{k} - \mathbf{k}') g_0^R(\mathbf{k}'s', E) \frac{1 + ss' \cos \theta}{2}, \quad (21)$$

where $g_0^R(\mathbf{k}'s', E) = (E - s' \hbar v_f k' + i0^+)^{-1}$ is the Green's function of the clean system and $\theta = \theta_{\mathbf{k}} - \theta_{\mathbf{k}'}$ is the angle between the wave vectors \mathbf{k} and \mathbf{k}' . We separate the calculation of the self-energy function into real and imaginary parts, by using Sokhotsky's formula, $\frac{1}{x+i0^+} = \mathcal{P}\frac{1}{x} - i\pi\delta(x)$, where \mathcal{P} denotes the Cauchy principal value.

The imaginary part of the self-energy can be solved as (details in Appendix C)

$$\text{Im}\Sigma^B(\mathbf{k}s, E) = -\frac{K_0}{4} |E| e^{-\frac{\xi^2}{2}(k^2 + \frac{E^2}{\hbar^2 v_f^2})} \times \left[I_0\left(\frac{\xi^2 k E}{\hbar v_f}\right) + s I_1\left(\frac{\xi^2 k E}{\hbar v_f}\right) \right], \quad (22)$$

where $I_0(x)$ and $I_1(x)$ are the zero and first order modified Bessel functions of the first kind [47,48]. Therefore, the real part of the self-energy is obtained as

$$\text{Re}\Sigma^B(\mathbf{k}s, E) = \frac{K_0}{4\pi} \mathcal{P} \int_{-E_c}^{E_c} dE' |E'| e^{-\frac{\xi^2}{2}(k^2 + \frac{E'^2}{\hbar^2 v_f^2})} \times \frac{I_0\left(\frac{\xi^2 k E'}{\hbar v_f}\right) + s I_1\left(\frac{\xi^2 k E'}{\hbar v_f}\right)}{E - E'}, \quad (23)$$

where E_c is the ultraviolet energy cutoff. Focusing on the Dirac physics ($\frac{|E|}{\hbar v_f}, k \ll \frac{1}{\xi}$), we expand the self-energy in powers of k and E ,

$$\begin{aligned} \text{Im}\Sigma^B(\mathbf{k}s, E) &= -\frac{K_0}{4} |E| + \dots, \\ \text{Re}\Sigma^B(\mathbf{k}s, E) &= \begin{cases} \frac{K_0}{2\pi} E \ln \left| \frac{E}{\hbar v_f k_c} \right| + \alpha E - s \alpha \hbar v_f k + \dots, & \xi \ll a, \\ \frac{K_0}{4\pi} E (\gamma + \ln \left| \frac{E \xi}{\hbar v_f} \right| - \ln 2) - s \alpha \hbar v_f k + \dots, & \xi \gg a, \end{cases} \end{aligned} \quad (24)$$

where $\gamma \approx 0.5772$ is the Euler-Mascheroni constant and \dots stands for terms in the order of $O(kE^2, k^2E, E^3)$ in the imaginary part and $O(kE^2 \ln E, k^2E \ln E, E^3 \ln E)$ in the real part and the dimensionless coefficient is

$$\alpha = \begin{cases} \frac{K_0 k_s^2 \xi^2}{8\pi}, & \xi \ll a, \\ \frac{K_0}{4\pi}, & \xi \gg a, \end{cases} \quad (25)$$

where K_0 is given by Eq. (7). This is quite consistent with the assumption Eq. (12) we set up in the previous section.

Here we stress that, in the literature, the Born approximation is widely applied together with the on-shell approximation, so that the momentum dependence of the self-energy is ignored [28,31]. Our findings show that in the low energy regime the on-shell approximation is not well justified, i.e., the momentum and energy dependence in the self-energy are decoupled as shown in Eqs. (24). We also show the derivation of the self-energy function in the high energy regime ($\frac{|E|}{\hbar v_f}, k \gg \frac{1}{\xi}$) in Appendix C, which arrives at

$$\text{Im}\Sigma^B(\mathbf{k}s, E) \approx -\frac{K_0(\hbar v_f)^2}{4\xi^2} \delta(E - E_{ks}), \quad (26)$$

$$\text{Re}\Sigma^B(\mathbf{k}s, E) \approx \frac{K_0(\hbar v_f)^2}{4\pi} \frac{E - E_{ks}}{\xi^2(E - E_{ks})^2 + (\hbar v_f)^2}. \quad (27)$$

It is obvious that the results in the condition $\frac{|E|}{\hbar v_f}, k \gg \frac{1}{\xi}$ can recover the on-shell approximation ($E = E_{ks}$). This result is further confirmed in the numerical simulation in Sec. IV D. Moreover, we find that the momentum-dependent terms are less important in the imaginary part of self-energy than those in the real part, since in the former they are at least two orders higher than the leading term.

2. Long-range screened Coulomb potential

Similar to the case of the long-ranged Gaussian potential, the self-energy function in the presence of the long-range screened Coulomb potential can be given by Eq. (21) with the correlation function $\mathcal{K}_G(\mathbf{k} - \mathbf{k}')$ replaced by $\mathcal{K}_C(\mathbf{k} - \mathbf{k}')$, so that

$$\Sigma^B(\mathbf{k}s, E) = \frac{1}{\mathcal{V}} \sum_{\mathbf{k}', s'} \frac{n_i V_0^2}{q_s^2 + k^2 + k'^2 - 2kk' \cos \theta} \times g_0^R(\mathbf{k}'s', E) \frac{1 + ss' \cos \theta}{2}. \quad (28)$$

Finally, we get the self-energy function in the presence of the long-range Coulomb potential based on the Born approximation with the low energy limit $k, \frac{E}{\hbar v_f} \ll q_s$, as

$$\begin{aligned} \text{Im}\Sigma(\mathbf{k}s, E) &= -\frac{n_i V_0^2}{4(\hbar v_f)^2 q_s^2} |E| + \dots, \\ \text{Re}\Sigma(\mathbf{k}s, E) &= \begin{cases} \frac{n_i V_0^2}{2\pi(\hbar v_f)^2 q_s^2} E \ln \left| \frac{E}{\hbar v_f k_c} \right| - \alpha \hbar v_f k + \dots, & q_s \gg \frac{1}{a}, \\ \frac{n_i V_0^2}{2\pi(\hbar v_f)^2 q_s^2} E \ln \left| \frac{E}{\hbar v_f q_s} \right| - \alpha \hbar v_f k + \dots, & q_s \ll \frac{1}{a}, \end{cases} \end{aligned} \quad (29)$$

with

$$\alpha = \begin{cases} \frac{n_i V_0^2 k_c^2}{2\pi(\hbar v_f)^2 q_s^4}, & q_s \gg \frac{1}{a}, \\ \frac{n_i V_0^2}{2\pi(\hbar v_f)^2 q_s^2}, & q_s \ll \frac{1}{a}. \end{cases} \quad (30)$$

Here \dots stands for terms in the order of $O(kE^2 \ln E, k^2E \ln E, E^3 \ln E)$ in the imaginary part and $O(kE^2 \ln E, k^2E \ln E, E^3 \ln E)$ in the real part.

It can be seen from the above results that the self-energy function of the long-range screened Coulomb potential has a similar expression as that of the long-ranged Gaussian potential, although the coefficient of the momentum-dependent term α is determined by the different parameters describing these two potentials. Physically, it can be understood from the following picture: around the Dirac point, the form of the random potential is not important, because the wavelength of the electron is longer than the spatial range of random potentials. So the different forms of random potentials give similar results, as we show in Eq. (24) and Eq. (29).

B. Self-consistent Born approximation (SCBA)

Furthermore, it should be noted that the Born approximation is essentially valid under weak disorder conditions ($K_0 \lesssim 1$) since it corresponds to the first order of the self-energy perturbation expansion. In this respect, one may wonder how the higher order expansions influence this calculation. We address it by taking the long-ranged Gaussian potential as an example and have also confirmed a momentum-dependent self-energy function by considering the self-consistent Born approximation (SCBA). Inspired by the Born approximation, we assume the self-energy function at the limit $k, \frac{E}{\hbar v_f} \ll \frac{1}{\xi}$ can be expressed in the form of

$$\Sigma(\mathbf{k}s, E) = \tilde{\Sigma}(E) - \alpha \hbar v_f k, \quad (31)$$

where $\tilde{\Sigma}(E) = \Sigma_1(E) + i\Sigma_2(E)$ is the part that depends only on energy. Then, the self-energy is assumed to be the solution of the self-consistent equation,

$$\begin{aligned} \tilde{\Sigma}(E) - \alpha \hbar v_f k &= \frac{1}{\mathcal{V}} \sum_{\mathbf{k}', s'} \mathcal{K}_G(\mathbf{k} - \mathbf{k}') \\ &\times \frac{1}{E - s'(1 - \alpha)\hbar v_f k' - \tilde{\Sigma}} \frac{1 + ss' \cos \theta}{2}. \end{aligned} \quad (32)$$

From the derivation presented in Appendix E, we find that the dimensionless parameter α , which controls the momentum linear dependent term in the self-energy, is given by

$$\alpha = \begin{cases} \frac{1}{2} - \sqrt{\frac{1}{4} - K_0 \frac{\xi^2 k_c^2}{8\pi}}, & \xi \ll a, \\ \frac{1}{2} - \sqrt{\frac{1}{4} - \frac{K_0}{4\pi}}, & \xi \gg a. \end{cases} \quad (33)$$

It is noticed that this result can recover to that obtained by the Born approximation, i.e., Eq. (24), at the weak disorder limit. Furthermore, the above result has an upper limit $\frac{1}{2}$. This implies that the coefficient α does not always increase with

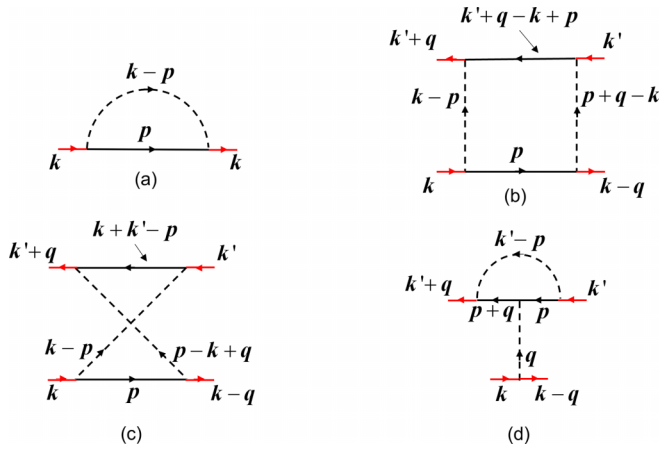


FIG. 2. One-loop RG diagrams responsible for the renormalization of (a) the energy and velocity and (b), (c), (d) the disorder coupling. Red lines denote external legs.

the increase of the disorder length scale and strength as given in the Born result. The fact that α has an upper limit is shown in the numerical simulations in Sec. IV D and shown in Fig. 5. In conclusion, we prove that the self-energy function is momentum dependent via the SCBA. More Feynman diagrams beyond the SCBA are hard to calculate, which will be further validated by the renormalization group analysis and numerical simulations.

C. One-loop renormalization group analysis

To further elucidate the above calculations, we perform a Wilson renormalization group analysis in the case of the long-ranged Gaussian potential. The purpose is twofold. First, the renormalization group analysis could help to clarify some effect beyond SCBA to the momentum-dependent self-energy function. Second, physically, the obtained flow equations clearly demonstrate the renormalized velocity together with the disorder coupling constant, which provides a different angle to understand our main conclusion.

At first, we expand the generating functional with cutoff prescription by setting the momentum ultraviolet cutoff Λ and disorder averaging:

$$\langle Z \rangle = \int D[\bar{\Psi}, \Psi]_{\Lambda} \exp \left[i \int dt d^2 \mathbf{x} \bar{\Psi}_{x,t} (i\partial_t + iv_f \nabla \cdot \boldsymbol{\sigma}) \Psi_{x,t} \right] \times \left\langle \exp \left[-i \int dt d^2 \mathbf{x} V(\mathbf{x}) \bar{\Psi}_{x,t} \Psi_{x,t} \right] \right\rangle. \quad (34)$$

According to Wilson's approach, we divide the field operator $\Psi(\mathbf{k})[\bar{\Psi}(\mathbf{k})]$ into two groups: $\Psi^{<}(\mathbf{k})[\bar{\Psi}^{<}(\mathbf{k})]$ for $[0, \Lambda/b]$ and $\Psi^{>}(\mathbf{k})[\bar{\Psi}^{>}(\mathbf{k})]$ $[\Lambda/b, \Lambda]$, where $b > 1$. Then, we can get the correction of the energy, momentum, and disorder coupling by integrating over $\Psi^{>}(\mathbf{k})[\bar{\Psi}^{>}(\mathbf{k})]$, whose one-loop Feynman diagrams are shown in Fig. 2. More derivations in detail are shown in Appendix F. Finally, after rescaling momentum and fields to keep the free propagator unchanged, the one-loop renormalization group equations of the running velocity \tilde{v}_f

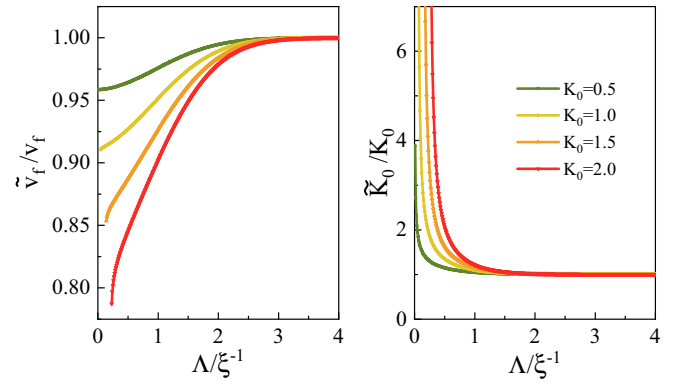


FIG. 3. One-loop RG flow of velocity \tilde{v}_f and disorder coupling \tilde{K}_0 .

and disorder coupling \tilde{K}_0 are given by

$$\begin{aligned} \frac{d\tilde{v}_f}{d \ln \Lambda} &= \frac{\tilde{K}_0 \xi^2 \Lambda^2}{4\pi} e^{-\frac{\xi^2 \Lambda^2}{2}} \tilde{v}_f, \\ \frac{d\tilde{K}_0}{d \ln \Lambda} &= -\frac{\tilde{K}_0^2}{\pi} e^{-\frac{\Lambda^2 \xi^2}{2}}, \end{aligned} \quad (35)$$

where the renormalization parameter is replaced by $d\Lambda = \Lambda/b - \Lambda \rightarrow b = 1 - d \ln \Lambda$.

In Fig. 3, we show the one-loop RG flow of velocity $\tilde{v}(\Lambda)$ and disorder coupling $\tilde{K}_0(\Lambda)$ by numerically solving Eq. (35) with starting points $\tilde{v}_f = v_f$ and $\tilde{v}_f = K_0$. As the momentum scale shrinks, equivalently, the real-space scale expands and the renormalized velocity decreases, which implies the parameter α characterizing the momentum-dependent part of the self-energy function is enhanced since the momentum-dependent part of the self-energy function in Eq. (12) effectively reduces velocity in energy dispersion. Moreover, the decrease of velocity positively related to K_0 . Furthermore, for $K_0 > 1$, the numerical results of the renormalized disorder coupling constant \tilde{K}_0 are extremely divergent, which also leads to a discontinuous behavior of the renormalized velocity. This implies the one-loop approximation may not be sufficient for a strong disorder potential.

Below we would like to provide some remarks. First, by setting $\xi \rightarrow 0$, the flow equations (35) go back to the existing results (e.g., Ref. [19]). That is, the renormalization of velocity is zero for short-ranged disorder potential. This is the main reason why the previous work overlooked the renormalization of velocity. Second, as we show here under the low energy condition ($k\xi, E\xi < 1$), a long-ranged fluctuation $\xi \neq 0$ leads to renormalization of the velocity. Importantly, the effective velocity is reduced under the renormalization group flow. Third, the renormalization group calculation is consistent with the calculation of the self-energy function, because the momentum-dependent part of the self-energy function, i.e., $\alpha \hbar v_f k$ in Eq. (12) and Eq. (24), effectively reduces velocity in the energy dispersion of electron. Taken all together, the independent renormalization group calculation further supports our conclusion.

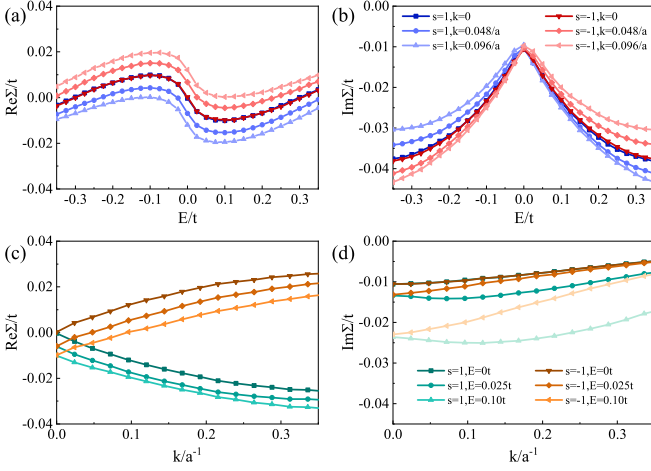


FIG. 4. Numerical results in the presence of the long-ranged Gaussian potential. (a),(b) Numerical results of E vs $\text{Re}\Sigma$ and E vs $\text{Im}\Sigma$ with different momenta k and band index s . (c),(d) Numerical results of k vs $\text{Re}\Sigma$ and k vs $\text{Im}\Sigma$ with different Fermi energies E and band index s . Here we set an impurity concentration $n_i = 5\%$, correlation length $\xi = 3.6a$, and impurity strength $u_0 = 0.16t$.

D. Numerical simulations

Above, we have derived the momentum dependence of the self-energy in the presence of long-range disorder potentials from the perturbation theories, which do not consider the

crossed Feynmann diagrams shown in Fig. 1(b). To further check these derivations, we next turn to numerical simulations. The Green's function $g(\mathbf{k}s, E)$ of the disordered system in the eigenbasis is directly calculated using the Lanczos recursive method [49] and the self-energy is obtained by the Dyson equation $\Sigma(\mathbf{k}s, E) = g_0^{-1}(\mathbf{k}s, E) - g^{-1}(\mathbf{k}s, E)$. In order to reach a high-energy resolution and reduce the finite-size errors, we consider a large supercell with $N = 2400 \times 2400 \times 2$ atoms. The data shown below are averaged over 50 random configurations.

1. Long-ranged Gaussian potential

In Fig. 4, we display the self-energy functions versus Fermi energy and momentum. Obviously, the self-energy depends not only on the Fermi energy, but also on the momentum. As shown in the $E - \text{Re}\Sigma$ plane of Fig. 4(a), the momentum dependence of the real part of the self-energy is significant in the low-energy region and gradually reduces with increasing energy, while the situation is opposite for the imaginary part shown in Fig. 4(b). From the curves in the $k - \text{Re}\Sigma$ plane in Fig. 4(c), we see that the real part of the self-energy near the Dirac point is linearly related to the momentum—positive for $s = -1$ and negative for $s = 1$. These behaviors mean that the estimation [Eq. (24)] without the on-shell approximation is reasonable around the Dirac point and therefore the self-energy in Eq. (12) is well justified.

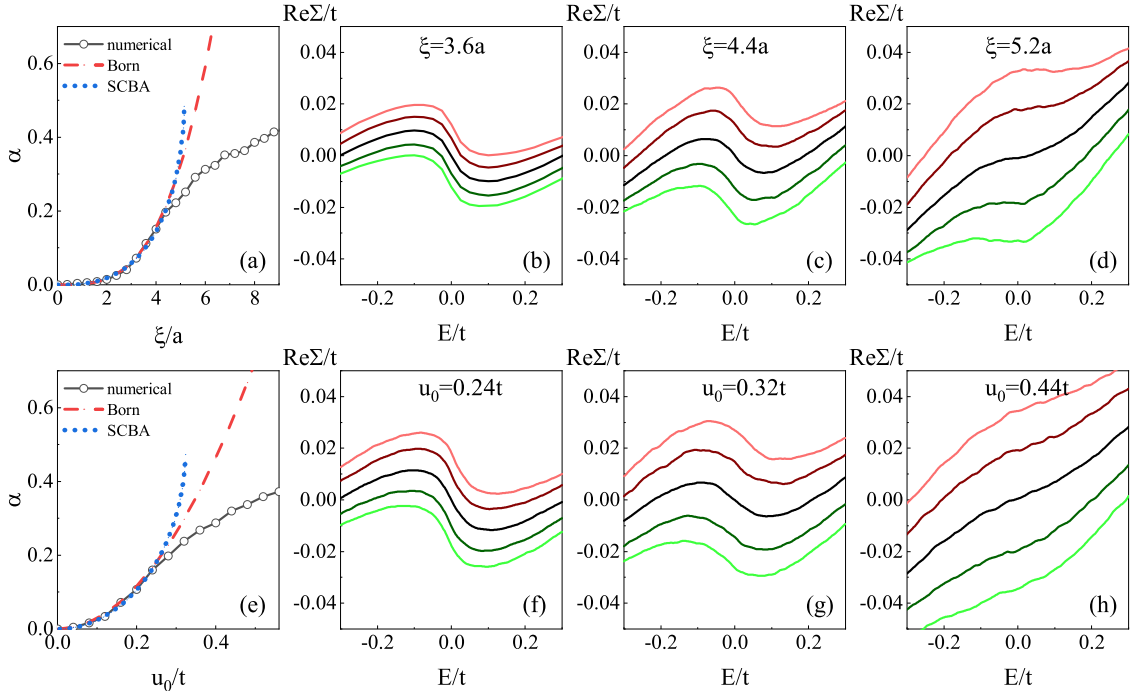


FIG. 5. Numerical results in the presence of the long-ranged Gaussian potential. (a) α versus ξ with $n_i = 5\%$ and $u_0 = 0.16t$. (b)–(d) Real part of the self-energy $\text{Re}\Sigma$ for different $\xi = 3.6a$ (b), $4.4a$ (c), and $5.2a$ (d). (e) α versus u_0 with $n_i = 5\%$ and $\xi = 3.2a$. (f)–(h) Real part of the self-energy $\text{Re}\Sigma$ for different $u_0 = 0.24t$ (f), $0.32t$ (g), and $0.44t$ (h). The dashed red lines (dotted blue lines) in (a),(e) are fitting curves based on the Born approximation, which have $\alpha = 1.6(\xi/a)^{3.3} \times 10^{-3}$ and $\alpha = 2.9(u_0/t)^2$. The dotted blue lines in (a),(e) are fitting curves based on the self-consistent Born approximation, which have $\alpha = \frac{1}{2} - \sqrt{\frac{1}{4} - 2.6(\xi/a)^{2.8} \times 10^{-3}}$ and $\alpha = \frac{1}{2} - \sqrt{\frac{1}{4} - 2.4(u_0/t)^2}$. In (b)–(d) and (f)–(h), the colors correspond to various momenta: Dirac point $k = 0$ (black), $k = 0.048/a$ and $s = -1$ (red), $k = 0.096/a$ and $s = -1$ (light red), $k = 0.048/a$ and $s = 1$ (green), and $k = 0.096/a$ and $s = 1$ (light green).

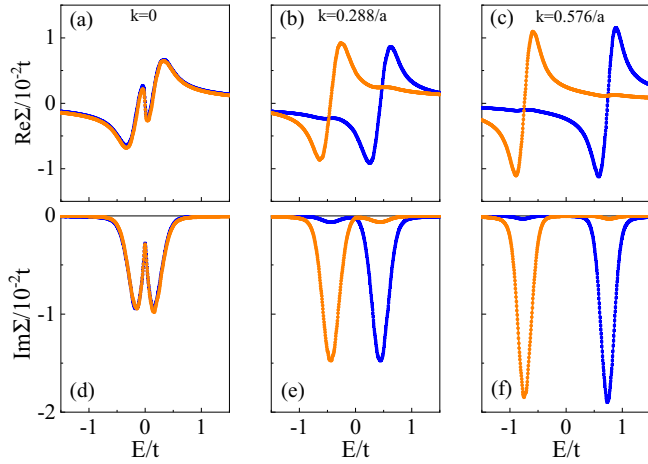


FIG. 6. Numerical results in the presence of the long-ranged Gaussian potential. (a)–(e) Numerical results of $\text{Re}\Sigma$ vs E with different momentum. (f)–(j) Numerical results of $\text{Im}\Sigma$ vs E . Blue lines denote subband with $s = 1$, while orange lines denote $s = -1$. Other parameters: impurity concentration $n_{\text{imp}} = 1\%$, correlation length $\xi = 10a$, and impurity strength $u_0 = 0.04t$.

Figures 5(a)–5(d) exhibit the effect of the correlation length ξ on the momentum dependence of the real part of the self-energy. The squares connected by solid line in Fig. 5(a) are the numerical results of parameter α versus correlation length ξ . When the disorder strength is small, α has a positive correlation with ξ , which can be fitted as $\alpha = 1.6(\xi/a)^{3.3} \times 10^{-3}$. This result is roughly consistent with the Born approximation which predicts $\alpha \propto \xi^2$ in the limit $\xi \ll a$ and $\alpha \propto \xi^4$ in the limit $\xi \gg a$ according to Eqs. (25) and (7). Upon increasing ξ , the value of α tends to saturate and eventually decreases. This behavior indicates that the Born approximation tends to be invalid away from the weak-scattering limit, since the increase of ξ also enhances the disorder strength K_0 .

Figures 5(f)–5(h) show the effect of the impurity strength u_0 . Similar to the correlation length, we fit the relation of ξ and α in the weak disorder regime and obtain $\alpha = 2.9(u_0/t)^2$. This result is in agreement with the prediction from the Born approximation: $\alpha \propto K_0 \propto u_0^2$. Equivalent to the ξ , a further increase of u_0 will also cause the system to enter the strong scattering limit. In addition, from Figs. 5(b)–5(d) and 5(f)–5(h), we find that the momentum dependence of the self-energy gradually decreases at high energy, where the on-shell approximation tends to be valid.

In Fig. 6, we further display the numerical simulation of the self-energy functions in the limit $k, \frac{E}{\hbar v_f} \gg \frac{1}{\xi}$ with impurity concentration $n_{\text{imp}} = 1\%$, correlation length $\xi = 10a$, and impurity strength $u_0 = 0.04t$. For the very small Fermi energy and momentum in Figs. 6(a) and 6(d), where the condition $k, E \ll \frac{1}{\xi}$ is still satisfied, the behavior of the real and imaginary parts of self-energy is qualitatively consistent with the results shown in Figs. 4(a) and 4(b). On the contrary, for the large Fermi energy and momentum, the imaginary part of self-energy tends to be a delta function which is the same as the prediction from Born approximation Eq. (26). Similarly, the numerical result of the real part of the self-energy is also consistent with the analytical expression Eq. (27).

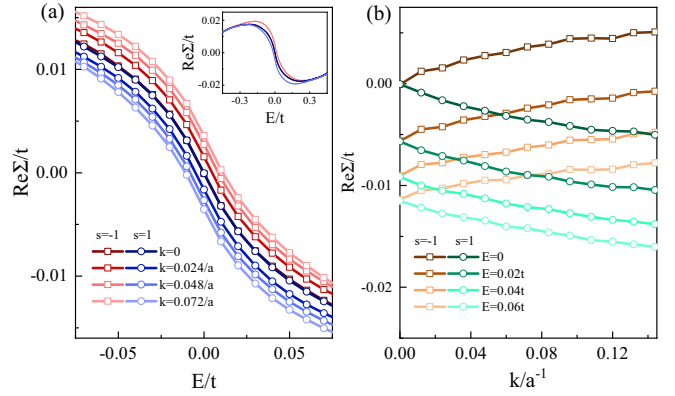


FIG. 7. Numerical results in the presence of the long-range screened Gaussian potential. (a) Numerical results of $\text{Re}\Sigma$ vs E . (b) Numerical results of $\text{Re}\Sigma$ vs k . Inset in (a) is the same as (a) but in a large energy range and only keeping the data of $k = 0$ and $k = 0.072/a$. Other parameters: $n_i = 0.05$, $V_0 = 0.1t$, and $q_s = 0.1a$. In order to avoid the divergence at $r \rightarrow 0$ in the discrete simulation, we set a minimum radius $r_c = 0.01a$.

2. Long-range screened Coulomb potential

In Sec. IV A 2, we have derived the self-energy function in the presence of long-range screened Coulomb potential based on the Born approximation. We also calculate it by numerical simulation. In Fig. 7, we show the numerical results of $\text{Re}\Sigma$ vs E and $\text{Re}\Sigma$ vs k near the Dirac point with parameters: $n_i = 0.05$, $V_0 = 0.1t$, and $q_s = 0.1a$. Additionally, in order to avoid the divergence at $r \rightarrow 0$ in the discrete simulation, we set a minimum radius $r_c = 0.01a$. Similar to the results in the presence of the long-ranged Gaussian potential in Figs. 4 and 5, the real part of the self-energy function shows linear dependence on the momentum, which is also consistent with that obtained from the Born approximation shown in Eq. (29).

V. DISCUSSION AND SUMMARY

We have shown that, in the presence of a long-ranged disorder potential, the self-energy function of the Dirac electrons has a peculiar dependence on the momentum and this momentum dependence is of paramount importance for the transport properties of graphene, i.e., it produces a nonuniversal minimal conductivity. Furthermore, we elaborate the origin of this momentum-dependent correction analytically and uncover its dependence on the disorder potential, which is also verified by unbiased numerical simulations.

In closing, we would like to make several remarks. First, our findings offer an intuitive way for understanding the existing numerical simulations where long-ranged impurities enhance the minimal conductivity. We believe that the physics behind these numerical calculations is now clear, from clarifying the self-energy function. Second, another main cautionary message is that the on-shell approximation is not well justified around the Dirac point. Third, both analytical and numerical results show that the on-shell approximation tends to be valid in the limit $k, \frac{E}{\hbar v_f} \gg \frac{1}{\xi}$, which means that in the high energy region the self-energy function becomes momentum independent, in line with previous theories. Fi-

nally, this work implies a consistent theory for the quantum transport of graphene: two main experimental observations, i.e., the linear dependence of the conductivity on carrier

density and the sample-dependent minimal conductivity, can be well understood by the presence of long-ranged impurity potentials.

ACKNOWLEDGMENTS

We thank M. Smidman for critical proofreading of the final version of the current manuscript. This work was supported by ‘‘Pioneer’’ and ‘‘Leading Goose’’ R&D Program of Zhejiang (Grant No. 2022SDXHDX0005), National Key R&D Program (Grant No. 2022YFA1402200), National Natural Science Foundation of China (Grants No. 12047544 and No. 11874337), and the foundation of Westlake University.

APPENDIX A: BUBBLE DIAGRAM OF KUBO FORMULA WITH MOMENTUM-DEPENDENT SELF-ENERGY

Here we present the calculation of the leading order of conductivity $\sigma_{xx}^{(0)}(E)$ based on the Kubo formula Eq. (13) with a general momentum-dependent self-energy Eq. (12). Considering the Green’s function and velocity in the eigenbasis of pseudospin, the leading order of the conductivity is given by

$$\sigma_{xx}^{(0)}(E) = \sigma_{xx}^{(0),RA}(E) - \text{Re}[\sigma_{xx}^{(0),RR}(E)], \quad (\text{A1})$$

with

$$\begin{aligned} \sigma_{xx}^{0,LM}(E) &= 4 \frac{e^2 \hbar}{2\pi \mathcal{V}} \text{Tr}[G^R(E) v_x G^A(E) v_x] \\ &= \frac{2e^2 \hbar v_f^2}{\pi} \int \frac{d^2 \mathbf{k}}{(2\pi)^2} \text{Tr} \left[\begin{pmatrix} g_+^L & 0 \\ 0 & g_-^L \end{pmatrix} \begin{pmatrix} \cos \theta_k & -i \sin \theta_k \\ i \sin \theta_k & -\cos \theta_k \end{pmatrix} \begin{pmatrix} g_+^M & 0 \\ 0 & g_-^M \end{pmatrix} \begin{pmatrix} \cos \theta_k & -i \sin \theta_k \\ i \sin \theta_k & -\cos \theta_k \end{pmatrix} \right] \\ &= \frac{2e^2 \hbar v_f^2}{\pi} \int \frac{d^2 \mathbf{k}}{(2\pi)^2} [\cos^2 \theta_k (g_+^L g_+^M + g_-^L g_-^M) + \sin^2 \theta_k (g_+^L g_-^M + g_-^L g_+^M)] \\ &= \frac{e^2 \hbar v_f^2}{2\pi^2} \int k dk (g_+^L g_+^M + g_-^L g_-^M + g_+^L g_-^M + g_-^L g_+^M), \end{aligned} \quad (\text{A2})$$

where $L = R, A$ denotes the retarded or advanced Green’s function and $g_{\pm}^{R/A}$ is the abbreviation of $g_{\pm}^{R/A}(\mathbf{k}, E)$.

In order to analyze the contribution of electron-hole coherence, we rewrite Eq. (A1) as

$$\sigma_{xx}^0(E) = \sigma_{xx}^{0,i}(E) + \sigma_{xx}^{0,c}(E), \quad (\text{A3})$$

with

$$\begin{aligned} \sigma_{xx}^{0,i}(E) &= \frac{e^2 \hbar v_f^2}{2\pi^2} \int k dk [g_+^R g_+^A + g_+^R g_+^A - \text{Re}(g_+^R g_+^R + g_-^R g_-^R)], \\ \sigma_{xx}^{0,c}(E) &= \frac{e^2 \hbar v_f^2}{\pi^2} \int k dk [g_+^R g_-^A - \text{Re}(g_+^R g_-^R)], \end{aligned} \quad (\text{A4})$$

where $\sigma_{xx}^{(0),i}(E)$ denotes the electron-hole incoherent contribution due to the product of the Green’s function with the same band index and $\sigma_{xx}^{(0),c}(E)$ denotes the electron-hole coherent contribution due to the product of the Green’s function with opposite band index. Plugging the Green’s function with a general self-energy in eigenbasis, i.e., Eq. (16), into the above equations, these two terms are given by

$$\begin{aligned} \sigma_{xx}^{0,i}(E) &= \frac{e^2 \hbar v_f^2}{2\pi^2} \text{Re} \int_0^\infty k dk \left\{ \frac{1}{[a - (1 - \alpha) \hbar v_f k + i\eta][a - (1 - \alpha) \hbar v_f k - i\eta]} + \frac{1}{[a + (1 - \alpha) \hbar v_f k + i\eta][a + (1 - \alpha) \hbar v_f k - i\eta]} \right. \\ &\quad \left. - \frac{1}{[a - (1 - \alpha) \hbar v_f k + i\eta][a - (1 - \alpha) \hbar v_f k + i\eta]} - \frac{1}{[a + (1 - \alpha) \hbar v_f k + i\eta][a + (1 - \alpha) \hbar v_f k + i\eta]} \right\} \\ &= \frac{2e^2}{\pi h (1 - \alpha)^2} \left(1 + \frac{a}{\eta} \arctan \frac{a}{\eta} \right) \end{aligned} \quad (\text{A5})$$

and

$$\begin{aligned} \sigma_{xx}^{0,c}(E) &= \frac{e^2 \hbar v_f^2}{\pi^2} \text{Re} \int_0^\infty k dk \left\{ \frac{1}{[a - (1 - \alpha) \hbar v_f k + i\eta][a + (1 - \alpha) \hbar v_f k - i\eta]} - \frac{1}{[a - (1 - \alpha) \hbar v_f k + i\eta][a + (1 - \alpha) \hbar v_f k + i\eta]} \right\} \\ &= \frac{2e^2}{\pi h (1 - \alpha)^2} \frac{\eta}{a} \arctan \frac{a}{\eta}. \end{aligned} \quad (\text{A6})$$

Thus the total conductivity obtained by the bubble diagram is

$$\sigma_{xx}^0(E) = \frac{2e^2}{\pi h} \frac{1}{(1-\alpha)^2} \left(1 + \frac{a}{\eta} \arctan \frac{a}{\eta}\right) + \frac{2e^2}{\pi h} \frac{1}{(1-\alpha)^2} \frac{\eta}{a} \arctan \frac{a}{\eta}, \quad (\text{A7})$$

which is Eq. (18) in the main text.

APPENDIX B: VERTEX CORRECTION OF KUBO FORMULA WITH MOMENTUM-DEPENDENT SELF-ENERGY

The vertex corrected dc conductivity as shown in Figs. 1(c) and 1(d), i.e., ladder diagrams, can be calculated by

$$\sigma_{xx}^v(E) = \sigma_{xx}^{v,RA}(E) - \text{Re}[\sigma_{xx}^{v,RR}(E)], \quad (\text{B1})$$

with

$$\sigma_{xx}^{v,RA}(E) = 4 \frac{e^2 \hbar}{2\pi} \int \frac{d^2 \mathbf{k}}{(2\pi)^2} \text{Tr}[G^R(\mathbf{k}, E) v_x(\mathbf{k}) G^A(\mathbf{k}, E) \tilde{v}_x^{RA}(\mathbf{k})], \quad (\text{B2})$$

$$\sigma_{xx}^{v,RR}(E) = 4 \frac{e^2 \hbar}{2\pi} \int \frac{d^2 \mathbf{k}}{(2\pi)^2} \text{Tr}[G^R(\mathbf{k}, E) v_x(\mathbf{k}) G^R(\mathbf{k}, E) \tilde{v}_x^{RR}(\mathbf{k})]. \quad (\text{B3})$$

Here, the ‘‘dressed’’ vertex function \tilde{v}_x^{LM} is defined by the self-consistent Bethe-Salpeter equation

$$\tilde{v}_x^{LM}(\mathbf{k}, E) = v_x(\mathbf{k}) + \int \frac{d^2 \mathbf{k}'}{(2\pi)^2} \mathcal{K}(\mathbf{k} - \mathbf{k}') U_{\mathbf{k}}^\dagger U_{\mathbf{k}'} G^L(\mathbf{k}', E) \tilde{v}_x^{LM}(\mathbf{k}', E) G^M(\mathbf{k}', E) U_{\mathbf{k}'}^\dagger U_{\mathbf{k}}, \quad (\text{B4})$$

where

$$U_{\mathbf{k}}^\dagger U_{\mathbf{k}'} = \frac{1}{2} \begin{pmatrix} 1 + e^{i\theta} & 1 - e^{i\theta} \\ 1 - e^{i\theta} & 1 + e^{i\theta} \end{pmatrix} \quad \text{with } \theta = \theta_{\mathbf{k}'} - \theta_{\mathbf{k}} \quad (\text{B5})$$

denotes the spin rotation as the momentum changes. In order to solve this self-consistent equation, we at first consider the first order approximation in the following:

$$\begin{aligned} \tilde{v}_x^{(1),LM}(\mathbf{k}, E) &= v_x(\mathbf{k}) + \int \frac{d^2 \mathbf{k}'}{(2\pi)^2} \mathcal{K}(\mathbf{k} - \mathbf{k}') U_{\mathbf{k}}^\dagger U_{\mathbf{k}'} G^L(\mathbf{k}', E) v_x(\mathbf{k}') G^M(\mathbf{k}', E) U_{\mathbf{k}'}^\dagger U_{\mathbf{k}} \\ &= v_x(\mathbf{k}) + v_f \int \frac{d^2 \mathbf{k}'}{(2\pi)^2} \frac{\mathcal{K}(\mathbf{k} - \mathbf{k}')}{4} \begin{pmatrix} 1 + e^{i\theta} & 1 - e^{i\theta} \\ 1 - e^{i\theta} & 1 + e^{i\theta} \end{pmatrix} \begin{pmatrix} g_+^L & \\ & g_-^L \end{pmatrix} \\ &\quad \times \begin{pmatrix} \cos \theta_{\mathbf{k}'} & -i \sin \theta_{\mathbf{k}'} \\ i \sin \theta_{\mathbf{k}'} & -\cos \theta_{\mathbf{k}'} \end{pmatrix} \begin{pmatrix} g_+^M & \\ & g_-^M \end{pmatrix} \begin{pmatrix} 1 + e^{-i\theta} & 1 - e^{-i\theta} \\ 1 - e^{-i\theta} & 1 + e^{-i\theta} \end{pmatrix} \\ &= v_x(\mathbf{k}) + v_f \int \frac{d^2 \mathbf{k}'}{(2\pi)^2} \frac{\mathcal{K}(\mathbf{k} - \mathbf{k}')}{4} \begin{pmatrix} M_{11} & M_{12} \\ M_{21} & M_{22} \end{pmatrix}, \end{aligned} \quad (\text{B6})$$

where the expressions of $M_{ss'}$ are

$$\begin{aligned} M_{11} &= 2 \cos \theta (g_+^L g_+^M - g_-^L g_-^M) \cos \theta_{\mathbf{k}} + [2 \cos^2 \theta (g_+^L g_+^M + g_-^L g_-^M) + 2 \sin^2 \theta (g_+^L g_-^M + g_-^L g_+^M)] \cos \theta_{\mathbf{k}}, \\ M_{22} &= 2 \cos \theta (g_+^L g_+^M - g_-^L g_-^M) \cos \theta_{\mathbf{k}} + [2 \cos^2 \theta (g_+^L g_+^M + g_-^L g_-^M) + 2 \sin^2 \theta (g_+^L g_-^M + g_-^L g_+^M)] (-\cos \theta_{\mathbf{k}}), \\ M_{12} &= 2i \cos \theta (g_+^L g_-^M - g_-^L g_+^M) \sin \theta_{\mathbf{k}} + [2 \cos^2 \theta (g_+^L g_+^M + g_-^L g_-^M) + 2 \sin^2 \theta (g_+^L g_-^M + g_-^L g_+^M)] (-i \sin \theta_{\mathbf{k}}), \\ M_{21} &= 2i \cos \theta (g_+^L g_-^M - g_-^L g_+^M) \sin \theta_{\mathbf{k}} + [2 \cos^2 \theta (g_+^L g_+^M + g_-^L g_-^M) + 2 \sin^2 \theta (g_+^L g_-^M + g_-^L g_+^M)] (i \sin \theta_{\mathbf{k}}). \end{aligned} \quad (\text{B7})$$

Based on the expressions of $M_{ss'}$, we can rewrite $\tilde{v}_x^{(1),LM}(\mathbf{k}, E)$ as

$$\frac{\tilde{v}_x^{(1),LM}(\mathbf{k}, E)}{v_f} = f_0^{LM}(\mathbf{k}, E) \cos \theta_{\mathbf{k}} \sigma_0 + f_x^{LM}(\mathbf{k}, E) \sin \theta_{\mathbf{k}} \sigma_x + f_y^{LM}(\mathbf{k}, E) \sin \theta_{\mathbf{k}} \sigma_y + f_z^{LM}(\mathbf{k}, E) \cos \theta_{\mathbf{k}} \sigma_z. \quad (\text{B8})$$

For $\tilde{v}_x^{(1),RA}(\mathbf{k}, E)$, the functions $f_i^{RA}(\mathbf{k}, E)$ with $(i = 0, x, y, z)$ are

$$\begin{aligned} f_0^{RA}(\mathbf{k}, E) &= \int \frac{d^2 \mathbf{k}'}{(2\pi)^2} \frac{\mathcal{K}(\mathbf{k} - \mathbf{k}')}{2} \cos \theta (g_+^R g_+^A - g_-^R g_-^A) \\ &\approx \frac{K_0 (\hbar v_f)^2}{8\pi^2} \int k' dk' d\theta \left[1 - \frac{\xi^2}{2} (k^2 + k'^2) + \xi^2 k k' \cos \theta \right] \cos \theta (g_+^R g_+^A - g_-^R g_-^A) \\ &\approx \frac{K_0 \xi^2 a}{4\pi (1-\alpha)^3 \hbar v_f} \ln \left(\frac{E_c^2}{a^2 + \eta^2} \right) k, \end{aligned} \quad (\text{B9})$$

$$\begin{aligned}
f_x^{RA}(\mathbf{k}, E) &= \int \frac{d^2\mathbf{k}'}{(2\pi)^2} \frac{\mathcal{K}(\mathbf{k}-\mathbf{k}')}{2} i \cos\theta(g_{0,+}^R g_{0,-}^A - g_{0,-}^R g_{0,+}^A) \\
&\approx \frac{K_0(\hbar v_f)^2}{8\pi^2} \int k' dk' d\theta \left[1 - \frac{\xi^2}{2}(k^2 + k'^2) + \xi^2 k k' \cos\theta \right] i \cos\theta(g_+^R g_-^A - g_-^R g_+^A) \\
&\approx \frac{K_0 \xi^2 \eta}{4\pi(1-\alpha)^3 \hbar v_f} \ln\left(\frac{E_c^2}{a^2 + \eta^2}\right) k,
\end{aligned} \tag{B10}$$

$$\begin{aligned}
f_y^{RA}(\mathbf{k}, E) = f_z^{RA}(\mathbf{k}, E) &= 1 + \int \frac{d^2\mathbf{k}'}{(2\pi)^2} \frac{\mathcal{K}(\mathbf{k}-\mathbf{k}')}{2} [\cos^2 \Delta\theta(g_+^L g_+^M + g_-^L g_-^M) + \sin^2 \Delta\theta(g_+^L g_-^M + g_-^L g_+^M)] \\
&\approx 1 + \frac{K_0(\hbar v_f)^2}{8\pi} \int k' dk' (g_+^L g_+^M + g_-^L g_-^M + g_+^L g_-^M + g_-^L g_+^M) \\
&\approx 1 + \frac{K_0}{4\pi(1-\alpha)^2} \left(\frac{a}{\eta} + \frac{\eta}{a}\right) \arctan \frac{a}{\eta}.
\end{aligned} \tag{B11}$$

For $\tilde{v}_x^{RR}(\mathbf{k}, E)$, the functions $f_i^{RR}(\mathbf{k}, E)$ with $(i = 0, x, y, z)$ are

$$\begin{aligned}
f_0^{RR}(\mathbf{k}, E) &= \int \frac{d^2\mathbf{k}'}{(2\pi)^2} \frac{\mathcal{K}(\mathbf{k}-\mathbf{k}')}{2} \cos\theta(g_+^R g_+^R - g_-^R g_-^R) \\
&\approx \frac{K_0(\hbar v_f)^2}{8\pi^2} \int k' dk' d\theta \left[1 - \frac{\xi^2}{2}(k^2 + k'^2) + \xi^2 k k' \cos\theta \right] \cos\theta(g_+^R g_+^R - g_-^R g_-^R) \\
&\approx \frac{K_0 \xi^2 (a + i\eta)}{4\pi(1-\alpha)^3 \hbar v_f} \ln\left(\frac{E_c^2}{a^2 + \eta^2}\right) k,
\end{aligned} \tag{B12}$$

$$f_x^{RR}(\mathbf{k}, E) = \int \frac{d^2\mathbf{k}'}{(2\pi)^2} \frac{\mathcal{K}(\mathbf{k}-\mathbf{k}')}{2} i \cos\theta(g_+^R g_-^R - g_-^R g_+^R) = 0, \tag{B13}$$

$$\begin{aligned}
f_y^{RR}(\mathbf{k}, E) = f_z^{RR}(\mathbf{k}, E) &= 1 + \int \frac{d^2\mathbf{k}'}{(2\pi)^2} \frac{\mathcal{K}(\mathbf{k}-\mathbf{k}')}{2} [\cos^2 \theta(g_+^R g_+^R + g_-^R g_-^R) + \sin^2 \theta(g_+^R g_-^R + g_-^R g_+^R)] \\
&\approx 1 + \frac{K_0(\hbar v_f)^2}{8\pi} \int k' dk' (g_+^R g_+^R + g_-^R g_-^R + g_+^R g_-^R + g_-^R g_+^R) \\
&\approx 1 - \frac{K_0}{4\pi(1-\alpha)^2}.
\end{aligned} \tag{B14}$$

Plugging Eqs. (B9)–(B14) into Eqs. (B8), (B2), and (B3), we can get the first-order $\sigma_{xx}^{v,RA}$ and $\text{Re}(\sigma_{xx}^{v,RR})$ as

$$\begin{aligned}
\sigma_{xx}^{(1),RA}(E) &= \frac{e^2 \hbar v_f^2}{2\pi^2} \int k dk \left[1 + \frac{K_0}{4\pi(1-\alpha)^2} \left(\frac{a}{\eta} + \frac{\eta}{a}\right) \arctan \frac{a}{\eta} \right] (g_+^R g_+^A + g_-^R g_-^A + g_+^R g_-^A + g_-^R g_+^A) \\
&\quad + \frac{K_0 \xi^2 a}{4\pi(1-\alpha)^3 \hbar v_f} \ln\left(\frac{E_c^2}{a^2 + \eta^2}\right) k (g_+^R g_+^A - g_-^R g_-^A) - i \frac{K_0 \xi^2 \eta}{4\pi(1-\alpha)^3 \hbar v_f} \ln\left(\frac{E_c^2}{a^2 + \eta^2}\right) k (g_+^R g_-^A - g_-^R g_+^A) \\
&= \frac{2e^2}{\pi h} \left\{ \left(\frac{a}{\eta} + \frac{\eta}{a}\right) \arctan \frac{a}{\eta} \left[1 + \frac{K_0}{4\pi(1-\alpha)^4} \left(\frac{a}{\eta} + \frac{\eta}{a}\right) \arctan \frac{a}{\eta} \right] + \frac{K_0 \xi^2 (a^2 - \eta^2)}{4\pi(\hbar v_f)^2} \left[\frac{1}{(1-\alpha)^3} \ln\left(\frac{E_c^2}{a^2 + \eta^2}\right) \right]^2 \right\}
\end{aligned} \tag{B15}$$

and

$$\begin{aligned}
\text{Re}[\sigma_{xx}^{(1),RR}(E)] &= \frac{e^2 \hbar v_f^2}{2\pi^2} \text{Re} \int k dk \left[1 - \frac{K_0}{4\pi(1-\alpha)^2} \right] (g_+^R g_+^R + g_-^R g_-^R + g_+^R g_-^R + g_-^R g_+^R) \\
&\quad + \frac{K_0 \xi^2 (a + i\eta)}{4\pi(1-\alpha)^3 \hbar v_f} \ln\left(\frac{E_c^2}{a^2 + \eta^2}\right) k (g_+^R g_+^R - g_-^R g_-^R) \\
&= \frac{2e^2}{\pi h} \left\{ -1 + \frac{K_0}{4\pi(1-\alpha)^4} + \frac{K_0 \xi^2 (a^2 - \eta^2)}{4\pi(\hbar v_f)^2} \left[\frac{1}{(1-\alpha)^3} \ln\left(\frac{E_c^2}{a^2 + \eta^2}\right) \right]^2 \right\},
\end{aligned} \tag{B16}$$

where $E_c = \hbar v_f k_c$. Thus the first-order vertex correction of dc conductivity is obtained as

$$\begin{aligned}\sigma_{xx}^{(1)}(E) &= \sigma_{xx}^{(1),RA}(E) - \text{Re}[\sigma_{xx}^{(1),RR}(E)] \\ &= \frac{2e^2}{\pi h} \left[1 + \left(\frac{a}{\eta} + \frac{\eta}{a} \right) \arctan \frac{a}{\eta} \right] + \frac{K_0}{4\pi(1-\alpha)^4} \left\{ \left[\left(\frac{a}{\eta} + \frac{\eta}{a} \right) \arctan \frac{a}{\eta} \right]^2 - 1 \right\},\end{aligned}\quad (\text{B17})$$

from which we can see that coefficients f_0^{LM} and f_x^{LM} can be ignored in the ‘‘dressed’’ vertex. Thus we can find that the dressed vertex has the same matrix structure with the bare velocity and can be solved as

$$\begin{aligned}\tilde{v}_x^{RA}(\mathbf{k}, E) &= \frac{1}{1 - \frac{K_0}{4\pi(1-\alpha)^2} \left(\frac{a}{\eta} + \frac{\eta}{a} \right) \arctan \frac{a}{\eta}} v_f (\cos \theta_k \sigma_z + \sin \theta_k \sigma_y), \\ \tilde{v}_x^{RR}(\mathbf{k}, E) &= \frac{1}{1 + \frac{K_0}{4\pi(1-\alpha)^2}} v_f (\cos \theta_k \sigma_z + \sin \theta_k \sigma_y).\end{aligned}\quad (\text{B18})$$

Based on this corrected vertex, the total dc conductivity will arrive at

$$\sigma_{xx}^v(E) = \frac{2e^2}{\pi h} \frac{1}{(1-\alpha)^2} \left[\frac{1}{1 + \frac{K_0}{4\pi(1-\alpha)^2}} + \frac{\left(\frac{a}{\eta} + \frac{\eta}{a} \right) \arctan \frac{a}{\eta}}{1 - \frac{K_0}{4\pi(1-\alpha)^2} \left(\frac{a}{\eta} + \frac{\eta}{a} \right) \arctan \frac{a}{\eta}} \right]\quad (\text{B19})$$

and the corresponding vertex corrected minimal conductivity is

$$\sigma_{\min}^v = \frac{4e^2}{\pi h} \frac{1}{(1-\alpha)^2} \frac{1}{1 - \left[\frac{K_0}{4\pi(1-\alpha)^2} \right]^2} \xrightarrow{K_0 \lesssim 1} \frac{4e^2}{\pi h} \frac{1}{(1-\alpha)^2}.\quad (\text{B20})$$

Since typical experiment conditions of high mobility graphene correspond to $K_0 \lesssim 1$, the influence of vertex correction to the minimal conductivity is much smaller than those induced by the linear momentum-dependent self-energy in the bubble diagram.

APPENDIX C: BORN APPROXIMATION OF THE SELF-ENERGY IN THE CASE OF THE LONG-RANGED GAUSSIAN POTENTIAL

In this section, we evaluate the self-energy function in the presence of long-ranged Gaussian potential by the Born approximation,

$$\Sigma(\mathbf{k}s, E) = \sum_{s'} \int \frac{d^2\mathbf{k}'}{(2\pi)^2} \mathcal{K}_G(\mathbf{k} - \mathbf{k}') g_0^R(\mathbf{k}'s', E) \frac{1 + ss' \cos \theta}{2},\quad (\text{C1})$$

which is Eq. (21) in the main paper. After plugging the correlation function Eq. (6) into this equation, it can be rewritten as

$$\Sigma^B(\mathbf{k}s, E) = K_0 (\hbar v_f)^2 \sum_{s'} \int \frac{d^2\mathbf{k}'}{(2\pi)^2} e^{-\frac{\xi^2(\mathbf{k}-\mathbf{k}')^2}{2}} g_0^R(\mathbf{k}'s', E) \frac{1 + ss' \cos \theta}{2}.\quad (\text{C2})$$

Next we will evaluate the real part and imaginary part separately.

For $E > 0$, the imaginary part of the self-energy is

$$\begin{aligned}\text{Im} \Sigma^B(\mathbf{k}s, E) &= K_0 (\hbar v_f)^2 \sum_{s'} \int \frac{d^2\mathbf{k}'}{(2\pi)^2} e^{-\frac{\xi^2(\mathbf{k}-\mathbf{k}')^2}{2}} \frac{1 + ss' \cos \theta}{2} [-\pi \delta(E - s' \hbar v_f k')] \\ &= -\frac{\pi K_0 \hbar v_f}{2} \sum_{s'} \int \frac{k' dk' d\theta}{(2\pi)^2} e^{-\frac{\xi^2(k^2+k'^2-2kk' \cos \theta)}{2}} (1 + ss' \cos \theta) \delta\left(\frac{E}{\hbar v_f} - s' k'\right) \\ &= -\frac{K_0}{8\pi} E e^{-\frac{\xi^2}{2}(k^2 + \frac{E^2}{\hbar^2 v_f^2})} \int_{-\pi}^{\pi} d\theta e^{\frac{\xi^2 k E}{\hbar v_f} \cos \theta} (1 + s \cos \theta) \\ &= -\frac{K_0}{4} E e^{-\frac{\xi^2}{2}(k^2 + \frac{E^2}{\hbar^2 v_f^2})} \left[I_0\left(\frac{\xi^2 k E}{\hbar v_f}\right) + s I_1\left(\frac{\xi^2 k E}{\hbar v_f}\right) \right],\end{aligned}\quad (\text{C3})$$

where $I_{0/1}(x)$ are modified Bessel functions of the first kind. Similarly, for $E < 0$, the imaginary part of the self-energy is

$$\begin{aligned}\text{Im} \Sigma^B(\mathbf{k}s, E) &= K_0 (\hbar v_f)^2 \sum_{s'} \int \frac{d^2\mathbf{k}'}{(2\pi)^2} e^{-\frac{\xi^2(\mathbf{k}-\mathbf{k}')^2}{2}} \frac{1 + ss' \cos \theta}{2} [-\pi \delta(E - s' \hbar v_f k')] \\ &= -\frac{\pi K_0 \hbar v_f}{2} \sum_{s'} \int \frac{k' dk' d\theta}{(2\pi)^2} e^{-\frac{\xi^2(k^2+k'^2-2kk' \cos \theta)}{2}} (1 + ss' \cos \theta) \delta\left(\frac{E}{\hbar v_f} - s' k'\right)\end{aligned}$$

$$\begin{aligned}
&= \frac{K_0}{8\pi} E e^{-\frac{\xi^2}{2}(k^2 + \frac{E^2}{\hbar^2 v_f^2})} \int_{-\pi}^{\pi} d\theta e^{-\frac{\xi^2 k E \cos \theta}{\hbar v_f}} (1 - s \cos \theta) \\
&= \frac{K_0}{4} E e^{-\frac{\xi^2}{2}(k^2 + \frac{E^2}{\hbar^2 v_f^2})} \left[I_0\left(-\frac{\xi^2 k E}{\hbar v_f}\right) - s I_1\left(-\frac{\xi^2 k E}{\hbar v_f}\right) \right]. \tag{C4}
\end{aligned}$$

Combining two conditions, we can get

$$\text{Im}\Sigma^B(\mathbf{k}s, E) = -\frac{K_0}{4} |E| e^{-\frac{\xi^2}{2}(k^2 + \frac{E^2}{\hbar^2 v_f^2})} \left[I_0\left(\frac{\xi^2 k E}{\hbar v_f}\right) + s I_1\left(\frac{\xi^2 k E}{\hbar v_f}\right) \right]. \tag{C5}$$

The corresponding real part of the self-energy function can be calculated by the Kramer-Kronig relation,

$$\text{Re}\Sigma^B(\mathbf{k}s, E) = \frac{1}{\pi} \mathcal{P} \int_{-E_c}^{E_c} dE' \frac{\text{Im}\Sigma^B(\mathbf{k}s, E')}{E' - E} = \frac{1}{\pi} \mathcal{P} \int_{-E_c}^{E_c} dE' \frac{-\frac{K_0}{4} |E'| e^{-\frac{\xi^2}{2}(k^2 + \frac{E'^2}{\hbar^2 v_f^2})} \left[I_0\left(\frac{\xi^2 k E'}{\hbar v_f}\right) + s I_1\left(\frac{\xi^2 k E'}{\hbar v_f}\right) \right]}{E' - E}. \tag{C6}$$

In the following, we evaluate the self-energy function in two limits: $k, \frac{E}{\hbar v_f} \ll \frac{1}{\xi}$ and $k, \frac{E}{\hbar v_f} \gg \frac{1}{\xi}$. Moreover, for the limit $k, \frac{E}{\hbar v_f} \ll \frac{1}{\xi}$, we will further consider the integral in Eq. (C6) into two conditions, $\xi \ll a$ and $\xi \gg a$, which compares the lattice constant with the scale of the disorder potential. When the potential approaches short range, the former one satisfies.

(i) For the limit $k, \frac{E}{\hbar v_f} \ll \frac{1}{\xi}$, the imaginary part of the self-energy function can be expanded as

$$\begin{aligned}
\text{Im}\Sigma^B(\mathbf{k}s, E) &= -\frac{K_0}{4} |E| \left[1 - \frac{\xi^2}{2} \left(k^2 + \frac{E^2}{\hbar^2 v_f^2} \right) + O(k^4, E^4, k^2 E^2) \right] \left[1 + s \frac{\xi^2 k E}{2\hbar v_f} + O(k^2 E^2) \right] \\
&= -\frac{K_0 |E|}{4} \left[1 - \frac{\xi^2}{2} \left(k^2 + \frac{E^2}{\hbar^2 v_f^2} \right) + \frac{s \xi^2 k E}{2\hbar v_f} \right] + O(k^4, E^4, k^2 E^2) \\
&= -\frac{K_0 |E|}{4} + O(k E^2, k^2 E, E^3), \tag{C7}
\end{aligned}$$

which is Eq. (17) in the main paper. The modified Bessel functions are expanded as $I_0(x) = 1 + \frac{x^2}{4} + o(x^3)$ and $I_1(x) = \frac{x}{2} + o(x^3)$. Meanwhile, the real part of the self-energy function is given by

$$\begin{aligned}
\text{Re}\Sigma^B(\mathbf{k}s, E) &= \frac{1}{\pi} \mathcal{P} \int_{-E_c}^{E_c} dE' \frac{-\frac{K_0}{4} |E'| e^{-\frac{\xi^2}{2}(k^2 + \frac{E'^2}{\hbar^2 v_f^2})} \left[I_0\left(\frac{\xi^2 k E'}{\hbar v_f}\right) + s I_1\left(\frac{\xi^2 k E'}{\hbar v_f}\right) \right]}{E' - E} \\
&= \frac{K_0}{4\pi} \mathcal{P} \left\{ \int_{-E_c}^0 dE' \frac{E' e^{-\frac{\xi^2}{2}(k^2 + \frac{E'^2}{\hbar^2 v_f^2})} \left[I_0\left(\frac{\xi^2 k E'}{\hbar v_f}\right) + s I_1\left(\frac{\xi^2 k E'}{\hbar v_f}\right) \right]}{E' - E} - \int_0^{E_c} dE' \frac{E' e^{-\frac{\xi^2}{2}(k^2 + \frac{E'^2}{\hbar^2 v_f^2})} \left[I_0\left(\frac{\xi^2 k E'}{\hbar v_f}\right) + s I_1\left(\frac{\xi^2 k E'}{\hbar v_f}\right) \right]}{E' - E} \right\} \\
&= \frac{K_0 \hbar v_f}{4\pi} \mathcal{P} \left\{ \int_0^{k_c} d\tilde{E}' \frac{\tilde{E}' e^{-\frac{(k^2 + E'^2)\xi^2}{2}} \left[I_0(\xi^2 k \tilde{E}') - s I_1(\xi^2 k \tilde{E}') \right]}{\tilde{E}' + \tilde{E}} - \int_0^{k_c} d\tilde{E}' \frac{\tilde{E}' e^{-\frac{(k^2 + E'^2)\xi^2}{2}} \left[I_0(\xi^2 k \tilde{E}') + s I_1(\xi^2 k \tilde{E}') \right]}{\tilde{E}' - \tilde{E}} \right\} \\
&= -\frac{K_0 \hbar v_f}{2\pi} \mathcal{P} \int_0^{k_c} d\tilde{E}' e^{-\frac{(k^2 + E'^2)\xi^2}{2}} \frac{\tilde{E}' I_0(\xi^2 k \tilde{E}') + s \tilde{E}'^2 I_1(\xi^2 k \tilde{E}')}{\tilde{E}'^2 - \tilde{E}^2} \\
&\approx -\frac{K_0 \hbar v_f}{2\pi} \mathcal{P} \int_0^{k_c} d\tilde{E}' e^{-\frac{E'^2 \xi^2}{2}} \frac{\tilde{E}' \tilde{E}' + s \tilde{E}'^2 \frac{\xi^2 k \tilde{E}'}{2}}{\tilde{E}'^2 - \tilde{E}^2}. \tag{C8}
\end{aligned}$$

Here, $\tilde{E} = \frac{E}{\hbar v_f}$, $\tilde{E}' = \frac{E'}{\hbar v_f}$, and $k_c = \frac{E_c}{\hbar v_f}$. Since $k_c \sim 1/a$, we can further separate this result into two different conditions, $\xi \ll a$ and $\xi \gg a$,

$$\text{Re}\Sigma^B(\mathbf{k}s, E) \approx \begin{cases} \frac{K_0}{2\pi} E \ln \left| \frac{E}{\hbar v_f k_c} \right| + \alpha E - \alpha \hbar v_f k, & \xi \ll a, \\ \frac{K_0}{4\pi} E (\gamma + \ln \left| \frac{E \xi}{\hbar v_f} \right| - \ln 2) - \alpha \hbar v_f k, & \xi \gg a, \end{cases} \tag{C9}$$

with

$$\alpha = \begin{cases} \frac{K_0 k_c^2 \xi^2}{8\pi}, & \xi \ll a, \\ \frac{K_0}{4\pi}, & \xi \gg a, \end{cases} \quad K_0 = \frac{n_i u_0^2}{(\hbar v_f)^2} \begin{cases} \frac{A_c}{2}, & \xi \ll a, \\ \frac{2\pi^2}{A_c} \xi^4, & \xi \gg a, \end{cases} \quad (C10)$$

where $\gamma \approx 0.5772$ is the Euler-Mascheroni constant.

(ii) For the limit $k, \frac{E}{\hbar v_f} \gg \frac{1}{\xi}$, the imaginary part of the self-energy function has the following asymptotic expression:

$$\begin{aligned} \text{Im}\Sigma^B(\mathbf{k}s, E) &= -\frac{K_0}{4}|E|e^{-\frac{\xi^2}{2}(k^2 + \frac{E^2}{\hbar^2 v_f^2})} e^{\frac{\xi^2 k|E|}{\hbar v_f}} \sqrt{\frac{\hbar v_f}{2\pi\xi^2 k|E|}} [1 + s \text{sgn}(E)] \\ &= -\frac{K_0}{4}|E|e^{-\frac{\xi^2}{2}(k - \frac{|E|}{\hbar v_f})^2} \sqrt{\frac{\hbar v_f}{2\pi\xi^2 k|E|}} [1 + s \text{sgn}(E)] \\ &\approx -\frac{K_0(\hbar v_f)^2}{4\xi^2} \delta(E - E_{ks}), \end{aligned} \quad (C11)$$

where $\text{sgn}(E)$ is sign function of E . The exponential decay term $e^{-\frac{\xi^2}{2}(k - \frac{|E|}{\hbar v_f})^2}$ and the term $[1 + s \text{sgn}(E)]$ in the above at the second equation imply that the on-shell approximation ($E = E_{ks} = s\hbar v_f k$) is valid in this condition based on the approximation $\lim_{\sigma \rightarrow 0} \frac{1}{\sqrt{2\pi\sigma}} \exp(-x^2/2\sigma) = \delta(x)$. In this condition, the modified Bessel functions $I_0(x)$ and $I_1(x)$ are approximated as

$$I_0(x \rightarrow \infty) = \frac{1}{\sqrt{2\pi|x|}} \exp[|x|] \left[1 + o\left(\frac{1}{|x|}\right) \right] \approx \frac{1}{\sqrt{2\pi|x|}} e^{|x|} \quad (C12)$$

and

$$I_1(x \rightarrow \infty) = \frac{\text{sgn}(x)}{\sqrt{2\pi|x|} \sqrt{1 + \frac{1}{x^2}}} \exp \left[-\text{arsinh}\left(\frac{1}{|x|}\right) + |x| \sqrt{1 + \frac{1}{x^2}} \right] \left[1 + o\left(\frac{1}{|x| \sqrt{1 + \frac{1}{|x|^2}}}\right) \right] \approx \frac{\text{sgn}(x)}{\sqrt{2\pi x}} e^{|x|}, \quad (C13)$$

where $I_0(x)$ is an even function and $I_1(x)$ is an odd function. The corresponding real part of the self-energy function is

$$\begin{aligned} \text{Re}\Sigma^B(\mathbf{k}s, E) &= \frac{1}{\pi} \mathcal{P} \int_{-\infty}^{\infty} dE' \frac{\text{Im}\Sigma^B(\mathbf{k}s, E')}{E' - E} \approx \frac{1}{\pi} \mathcal{P} \int_{-\infty}^{\infty} dE' \frac{-\frac{K_0(\hbar v_f)^2}{4\xi^2} \delta(E' - E_{ks})}{E' - E} \\ &= -\frac{K_0(\hbar v_f)^2}{4\xi^2} \frac{1}{\pi} \mathcal{P} \int_{-\infty}^{\infty} dE' \frac{\delta(E' - E_{ks})}{E' - E_{ks} - (E - E_{ks})} = -\frac{K_0(\hbar v_f)^2}{4\xi^2} \frac{1}{\pi} \mathcal{P} \int_{-\infty}^{\infty} d\omega \frac{\delta(\omega)}{\omega - (E - E_{ks})} \\ &= -\frac{K_0(\hbar v_f)^2}{4\xi^2} \frac{1}{2\pi} \mathcal{P} \left[\int_{-\infty}^{\infty} d\omega \frac{\delta(\omega)}{\omega - (E - E_{ks})} + \int_{-\infty}^{\infty} d\omega \frac{\delta(\omega)}{-\omega - (E - E_{ks})} \right] \\ &\approx -\frac{K_0(\hbar v_f)^2}{4\xi^2} \frac{1}{2\pi} \int_{-\infty}^{\infty} d\omega \frac{2(E - E_{ks})\delta(\omega)}{\omega^2 - (E - E_{ks})^2 - (\hbar v_f/\xi)^2} = \frac{K_0(\hbar v_f)^2}{4\pi} \frac{E - E_{ks}}{\xi^2(E - E_{ks})^2 + (\hbar v_f)^2}, \end{aligned} \quad (C14)$$

where we introduced a quantity $\hbar v_f/\xi$ to simulate the broadening of the delta function and smear the divergence at the point $E = E_{ks}$.

To sum up, we obtain the self-energy function in two different regimes.

For $\frac{|E|}{\hbar v_f}, k \ll \frac{1}{\xi}$

$$\text{Im}\Sigma^B(\mathbf{k}s, E) = -\frac{K_0}{4}|E| + O(kE^2, k^2E, E^3), \quad (C15)$$

$$\text{Re}\Sigma^B(\mathbf{k}s, E) = \begin{cases} \frac{K_0}{2\pi} E \ln \left| \frac{E}{\hbar v_f k_c} \right| + \alpha E - s\alpha \hbar v_f k + O(kE^2 \ln E, k^2E \ln E, E^3 \ln E), & \xi \ll a, \\ \frac{K_0}{4\pi} E (\gamma + \ln \left| \frac{E\xi}{\hbar v_f} \right| - \ln 2) - s\alpha \hbar v_f k + O(kE^2 \ln E, k^2E \ln E, E^3 \ln E), & \xi \gg a, \end{cases} \quad (C16)$$

with

$$\alpha = \begin{cases} \frac{K_0 k_c^2 \xi^2}{8\pi}, & \xi \ll a, \\ \frac{K_0}{4\pi}, & \xi \gg a, \end{cases} \quad K_0 = \frac{n_i u_0^2}{(\hbar v_f)^2} \begin{cases} \frac{A_c}{2}, & \xi \ll a, \\ \frac{2\pi^2}{A_c} \xi^4, & \xi \gg a. \end{cases} \quad (C17)$$

For $k, \frac{E}{\hbar v_f} \gg \frac{1}{\xi}$,

$$\text{Im}\Sigma^B(\mathbf{k}s, E) \approx -\frac{K_0(\hbar v_f)^2}{4\xi^2} \delta(E - E_{ks}), \quad (\text{C18})$$

$$\text{Re}\Sigma^B(\mathbf{k}s, E) \approx \frac{K_0(\hbar v_f)^2}{4\pi} \frac{E - E_{ks}}{\xi^2(E - E_{ks})^2 + (\hbar v_f)^2}. \quad (\text{C19})$$

While the results in the condition $\frac{|E|}{\hbar v_f}, k \gg \frac{1}{\xi}$ can recover the on-shell approximation ($E = E_{ks}$), those in the condition $\frac{|E|}{\hbar v_f}, k \ll \frac{1}{\xi}$ are the main result of this work.

APPENDIX D: BORN APPROXIMATION OF THE SELF-ENERGY IN THE CASE OF THE LONG-RANGE SCREENED COULOMB POTENTIAL

Similar to the long-ranged Gaussian potential, the self-energy of long-range screened Coulomb potential based on the Born approximation is given by

$$\Sigma^B(\mathbf{k}s, E) = \sum_{s'} \int \frac{d^2\mathbf{k}'}{(2\pi)^2} \frac{n_i V_0^2}{q_s^2 + k^2 + k'^2 - 2kk' \cos \theta} g_0^R(\mathbf{k}'s', E) \frac{1 + ss' \cos \theta}{2}, \quad (\text{D1})$$

where N_i and $n_i = N_i/\mathcal{V}$ are the number and concentration of impurities and $V_0 = \frac{2\pi e^2}{\kappa}$.

For $E > 0$, the imaginary part of the self-energy is obtained as

$$\begin{aligned} \text{Im}\Sigma^B(\mathbf{k}s, E) &= \sum_{s'} \int \frac{d^2\mathbf{k}'}{(2\pi)^2} \frac{n_i V_0^2}{q_s^2 + k^2 + k'^2 - 2kk' \cos \theta} \frac{1 + ss' \cos \theta}{2} [-\pi \delta(E - s' \hbar v_f k')] \\ &= -\frac{\pi n_i V_0^2}{2} \int \frac{k' dk' d\theta}{(2\pi)^2} \frac{1 + s \cos \theta}{q_s^2 + k^2 + k'^2 - 2kk' \cos \theta} \delta(E - \hbar v_f k') = -\frac{n_i V_0^2 \tilde{E}}{8\pi \hbar v_f} \int d\theta \frac{1 + s \cos \theta}{q_s^2 + k^2 + \tilde{E}^2 - 2k\tilde{E} \cos \theta} \\ &= -\frac{n_i V_0^2 \tilde{E}}{8\pi \hbar v_f} \left(-\frac{1}{2k\tilde{E}} \right) \int d\theta \frac{s(q_s^2 + k^2 + \tilde{E}^2 - 2k\tilde{E} \cos \theta) - [s(q_s^2 + k^2 + \tilde{E}^2) + 2k\tilde{E}]}{q_s^2 + k^2 + \tilde{E}^2 - 2k\tilde{E} \cos \theta} \\ &= \frac{n_i V_0^2}{16\pi \hbar v_f k} \left\{ 2\pi s - [s(q_s^2 + k^2 + \tilde{E}^2) + 2k\tilde{E}] \int d\theta \frac{1}{q_s^2 + k^2 + \tilde{E}^2 - 2k\tilde{E} \cos \theta} \right\} \\ &= \frac{n_i V_0^2}{8\hbar v_f k} \left[s - \frac{s(q_s^2 + k^2 + \tilde{E}^2) + 2k\tilde{E}}{\sqrt{(q_s^2 + k^2 + \tilde{E}^2 - 2k\tilde{E})(q_s^2 + k^2 + \tilde{E}^2 + 2k\tilde{E})}} \right] = \frac{n_i V_0^2}{8\hbar v_f k} s \left[1 - \sqrt{\frac{q_s^2 + (k + s\tilde{E})^2}{q_s^2 + (k - s\tilde{E})^2}} \right] \\ &= \frac{n_i V_0^2}{8\hbar v_f k} s \left[1 - \sqrt{1 + \frac{4sk\tilde{E}}{q_s^2 + (k - s\tilde{E})^2}} \right] \approx -\frac{n_i V_0^2}{4\hbar v_f} \frac{\tilde{E}}{q_s^2 + (k - s\tilde{E})^2}, \quad (\text{D2}) \end{aligned}$$

where $\tilde{E} = \frac{E}{\hbar v_f}$, and we approximate the above equation at the limit $k, \tilde{E} \ll q_s^2$.

For $E < 0$, the imaginary part of the self-energy is

$$\begin{aligned} \text{Im}\Sigma^B(\mathbf{k}s, E) &= \sum_{s'} \int \frac{d^2\mathbf{k}'}{(2\pi)^2} \frac{n_i V_0^2}{q_s^2 + k^2 + k'^2 - 2kk' \cos \theta} \frac{1 + ss' \cos \theta}{2} [-\pi \delta(E - s' \hbar v_f k')] \\ &= -\frac{\pi n_i V_0^2}{2} \int \frac{k' dk' d\theta}{(2\pi)^2} \frac{1 - s \cos \theta}{q_s^2 + k^2 + k'^2 - 2kk' \cos \theta} \delta(E + \hbar v_f k') = \frac{n_i V_0^2 \tilde{E}}{8\pi \hbar v_f} \int d\theta \frac{1 - s \cos \theta}{q_s^2 + k^2 + \tilde{E}^2 + 2k\tilde{E} \cos \theta} \\ &= \frac{n_i V_0^2 \tilde{E}}{8\pi \hbar v_f} \left(\frac{1}{2k\tilde{E}} \right) \int d\theta \frac{-s(q_s^2 + k^2 + \tilde{E}^2 + 2k\tilde{E} \cos \theta) + [s(q_s^2 + k^2 + \tilde{E}^2) + 2k\tilde{E}]}{q_s^2 + k^2 + \tilde{E}^2 + 2k\tilde{E} \cos \theta} \\ &= \frac{n_i V_0^2}{16\pi \hbar v_f k} \left\{ -2\pi s + [s(q_s^2 + k^2 + \tilde{E}^2) + 2k\tilde{E}] \int d\theta \frac{1}{q_s^2 + k^2 + \tilde{E}^2 + 2k\tilde{E} \cos \theta} \right\} \\ &= -\frac{n_i V_0^2}{8\hbar v_f k} \left[s - \frac{s(q_s^2 + k^2 + \tilde{E}^2) + 2k\tilde{E}}{\sqrt{(q_s^2 + k^2 + \tilde{E}^2 - 2k\tilde{E})(q_s^2 + k^2 + \tilde{E}^2 + 2k\tilde{E})}} \right] = -\frac{n_i V_0^2}{8\hbar v_f k} s \left[1 - \sqrt{\frac{q_s^2 + (k + s\tilde{E})^2}{q_s^2 + (k - s\tilde{E})^2}} \right] \\ &= -\frac{n_i V_0^2}{8\hbar v_f k} s \left[1 - \sqrt{1 + \frac{4sk\tilde{E}}{q_s^2 + (k - s\tilde{E})^2}} \right] \approx \frac{n_i V_0^2}{4\hbar v_f} \frac{\tilde{E}}{q_s^2 + (k - s\tilde{E})^2}. \quad (\text{D3}) \end{aligned}$$

Combining two conditions, we can get

$$\text{Im}\Sigma^B(\mathbf{k}s, E) = -\frac{n_i V_0^2}{4\hbar v_f} \frac{|\tilde{E}|}{q_s^2 + (k - s\tilde{E})^2}. \quad (\text{D4})$$

Then the corresponding real part of the self-energy function can be calculated by the Kramer-Kronig relation

$$\begin{aligned} \text{Re}\Sigma^B(\mathbf{k}s, E) &= \frac{1}{\pi} \mathcal{P} \int_{-E_c}^{E_c} dE' \frac{\text{Im}\Sigma(\mathbf{k}s, E')}{E' - E} = -\frac{n_i V_0^2}{4\pi\hbar v_f} \int_{-E_c}^{E_c} d\tilde{E}' \frac{1}{\tilde{E}' - \tilde{E}} \frac{|\tilde{E}'|}{q_s^2 + (k - s\tilde{E}')^2} \\ &= -\frac{n_i V_0^2}{4\pi\hbar v_f} \left\{ \int_0^{\tilde{E}_c} d\tilde{E}' \frac{\tilde{E}'}{(\tilde{E}' - \tilde{E})[q_s^2 + (k - s\tilde{E}')^2]} + \int_{-\tilde{E}_c}^0 d\tilde{E}' \frac{-\tilde{E}'}{(\tilde{E}' - \tilde{E})[q_s^2 + (k - s\tilde{E}')^2]} \right\} \\ &= -\frac{n_i V_0^2}{4\pi\hbar v_f} \left\{ \int_0^{\tilde{E}_c} d\tilde{E}' \frac{\tilde{E}'}{(\tilde{E}' - \tilde{E})[q_s^2 + (k - s\tilde{E}')^2]} + \int_0^{\tilde{E}_c} d\tilde{E}' \frac{\tilde{E}'}{(-\tilde{E}' - \tilde{E})[q_s^2 + (k + s\tilde{E}')^2]} \right\} \\ &= -\frac{n_i V_0^2}{4\pi\hbar v_f} \int_0^{\tilde{E}_c} d\tilde{E}' \left\{ \frac{\tilde{E}'}{(\tilde{E}' - \tilde{E})[q_s^2 + (k - s\tilde{E}')^2]} - \frac{\tilde{E}'}{(\tilde{E}' + \tilde{E})[q_s^2 + (k + s\tilde{E}')^2]} \right\} \\ &\approx -\frac{n_i V_0^2}{4\pi(\hbar v_f)^2 q_s^2} \left[E \ln \frac{k_c^2 q_s^2}{\tilde{E}^2 (k_c^2 + q_s^2)} + \frac{2k_c^2}{k_c^2 + q_s^2} s\hbar v_f k \right], \end{aligned} \quad (\text{D5})$$

where $E_c = \hbar v_f k_c$.

Similar to the case of long-range Gaussian potential discussed in Appendix C, we can further separate this result into two different conditions, $q_s \ll \frac{1}{a}$ and $q_s \gg \frac{1}{a}$, where a denotes the lattice constant and $\frac{1}{a} \sim k_c$. Finally, we get the self-energy function in the presence of long-range Coulomb potential based on the Born approximation with the low energy limit $k, \frac{E}{\hbar v_f} \ll q_s$, as

$$\text{Im}\Sigma(\mathbf{k}s, E) = -\frac{n_i V_0^2}{4(\hbar v_f)^2 q_s^2} |E| + O(kE^2 \ln E, k^2 E \ln E, E^3 \ln E), \quad (\text{D6})$$

$$\text{Re}\Sigma(\mathbf{k}s, E) = \begin{cases} \frac{n_i V_0^2}{2\pi(\hbar v_f)^2 q_s^2} E \ln \left| \frac{E}{\hbar v_f k_c} \right| - \alpha \hbar v_f k + O(kE^2 \ln E, k^2 E \ln E, E^3 \ln E), & q_s \gg \frac{1}{a}, \\ \frac{n_i V_0^2}{2\pi(\hbar v_f)^2 q_s^2} E \ln \left| \frac{E}{\hbar v_f q_s} \right| - \alpha \hbar v_f k + O(kE^2 \ln E, k^2 E \ln E, E^3 \ln E), & q_s \ll \frac{1}{a}, \end{cases} \quad (\text{D7})$$

with

$$\alpha = \begin{cases} \frac{n_i V_0^2 k_c^2}{2\pi(\hbar v_f)^2 q_s^4}, & q_s \gg \frac{1}{a}, \\ \frac{n_i V_0^2}{2\pi(\hbar v_f)^2 q_s^2}, & q_s \ll \frac{1}{a}. \end{cases} \quad (\text{D8})$$

APPENDIX E: SCBA OF THE SELF-ENERGY FUNCTION IN THE CASE OF THE LONG-RANGED GAUSSIAN POTENTIAL

Inspired by the Born approximation, we assume the self-energy function at the limit $k, \frac{E}{\hbar v_f} \ll \frac{1}{\xi}$ can be expressed in the form of

$$\Sigma(\mathbf{k}s, E) = \Sigma_1(E) - \alpha \hbar v_f k + i\Sigma_2(E) = \tilde{\Sigma}(E) - \alpha \hbar v_f k, \quad (\text{E1})$$

where $\tilde{\Sigma}(E) = \Sigma_1(E) + i\Sigma_2(E)$ is the part that depends only on energy. Thus the self-energy function based on the SCBA Feynman diagram at the limit $k, \frac{E}{\hbar v_f} \ll \frac{1}{\xi}$ is given by

$$\begin{aligned} \Sigma(\mathbf{k}s, E) &= \sum_{s'} \int \frac{d^2\mathbf{k}'}{(2\pi)^2} \mathcal{K}(\mathbf{k} - \mathbf{k}') G(\mathbf{k}'s', E) \frac{1 + ss' \cos \theta}{2} \\ &= K_0 (\hbar v_f)^2 \sum_{s'} \int \frac{d^2\mathbf{k}'}{(2\pi)^2} e^{-\frac{\xi^2(\mathbf{k}-\mathbf{k}')^2}{2}} \frac{1}{E - E_{\mathbf{k}'s'} - \Sigma(\mathbf{k}'s', E)} \frac{1 + ss' \cos \theta}{2} \\ &= K_0 (\hbar v_f)^2 \sum_{s'} \int \frac{d^2\mathbf{k}'}{(2\pi)^2} e^{-\frac{\xi^2(\mathbf{k}-\mathbf{k}')^2}{2}} \frac{1}{E - s'(1 - \alpha)\hbar v_f k' - \tilde{\Sigma}} \frac{1 + ss' \cos \theta}{2} \\ &= \frac{K_0 (\hbar v_f)^2}{2} \int \frac{k' dk' d\theta}{(2\pi)^2} e^{-\frac{\xi^2(\mathbf{k}-\mathbf{k}')^2}{2}} \left[\frac{1 + s \cos \theta}{(E - \tilde{\Sigma}) - (1 - \alpha)\hbar v_f k'} + \frac{1 - s \cos \theta}{(E - \tilde{\Sigma}) + (1 - \alpha)\hbar v_f k'} \right] \end{aligned}$$

$$\begin{aligned}
&= \frac{K_0(\hbar v_f)^2}{2\pi^2} \int_0^{k_c} k' dk' \int_0^\pi d\theta e^{-\frac{\xi^2(k^2+k'^2-2kk'\cos\theta)}{2}} \frac{(E - \tilde{\Sigma}) + s \cos\theta(1 - \alpha)\hbar v_f k'}{(E - \tilde{\Sigma})^2 - (1 - \alpha)^2(\hbar v_f k')^2} \\
&= \frac{K_0(\hbar v_f)^2}{2\pi} \int_0^{k_c} k' dk' e^{-\frac{\xi^2(k^2+k'^2)}{2}} \left[\frac{(E - \tilde{\Sigma})}{(E - \tilde{\Sigma})^2 - (1 - \alpha)^2(\hbar v_f k')^2} I_0(kk'\xi^2) \right. \\
&\quad \left. + \frac{s(1 - \alpha)\hbar v_f k'}{(E - \tilde{\Sigma})^2 - (1 - \alpha)^2(\hbar v_f k')^2} I_1(kk'\xi^2) \right] \\
&= \frac{K_0(\hbar v_f)^2}{2\pi} \int_0^{k_c} k' dk' [1 + o(k^2\xi^2)] e^{-\frac{\xi^2 k'^2}{2}} \frac{(E - \tilde{\Sigma})[1 + o(k^2\xi^2)] + s(1 - \alpha)\hbar v_f k' [\frac{kk'\xi^2}{2} + o(k^2\xi^2)]}{(E - \tilde{\Sigma})^2 - (1 - \alpha)^2(\hbar v_f k')^2} \\
&\approx \frac{K_0(\hbar v_f)^2}{2\pi} \int_0^{k_c} k' dk' \frac{(E - \tilde{\Sigma})e^{-\frac{\xi^2 k'^2}{2}}}{(E - \tilde{\Sigma})^2 - (1 - \alpha)^2(\hbar v_f k')^2} + s(1 - \alpha)\hbar v_f k \frac{\frac{\xi^2 k'^2}{2} e^{-\frac{\xi^2 k'^2}{2}}}{(E - \tilde{\Sigma})^2 - (1 - \alpha)^2(\hbar v_f k')^2} \\
&= \frac{K_0}{4\pi(1 - \alpha)^2} \left[(E - \tilde{\Sigma})e^{-(E - \tilde{\Sigma})^2 \xi^2} (\text{Ei}[(E - \tilde{\Sigma})^2 \xi^2] - \text{Ei}[(E - \tilde{\Sigma})^2 \xi^2 - \Lambda^2 \xi^2]) - s(1 - \alpha)\hbar v_f k (1 - e^{-\Lambda^2 \xi^2}) \right. \\
&\quad \left. + s(1 - \alpha)\hbar v_f k (E - \tilde{\Sigma})^2 \xi^2 e^{-(E - \tilde{\Sigma})^2 \xi^2} (\text{Ei}[(E - \tilde{\Sigma})^2 \xi^2] - \text{Ei}[(E - \tilde{\Sigma})^2 \xi^2 - \Lambda^2 \xi^2]) \right], \tag{E2}
\end{aligned}$$

where $\tilde{\xi}^2 = \frac{\xi^2}{2(\hbar v_f)^2(1 - \alpha)^2}$, $\tilde{k} = s(1 - \alpha)E_c$, $E_c = \hbar v_f k_c$, and $\Lambda = (1 - \alpha)(\hbar v_f k_c)$. $\text{Ei}(x)$ is an exponential integral function. The first term in square brackets is consistent with the short-range disorder when assuming $\alpha \rightarrow 0$ and $\xi \rightarrow 0$, which can be solved in two limits $|E| \ll \Gamma_0$ and $|E| \gg \Gamma_0$. $\Gamma_0 = E_c e^{-2\pi/K_0}$ is an exponential small energy scale defined by the imaginary part of self-energy at the Dirac point [19]. Similarly, in the following, we will solve this self-consistent equation in two limits: $|E| \ll \Gamma_0$ and $|E| \gg \Gamma_0$. According to the Born results [Eqs. (C15) and (C16)], in the case of the long-range potential, it is necessary to further consider two conditions, $\xi \ll a$ and $\xi \gg a$, which compare the lattice constant with the scale of the disorder potential. When the potential approaches short range, the former one satisfies.

To sum up, we obtain the self-energy function based on SCBA as follows.

1. $\xi \ll a$

At this limit, Eq. (E2) is reduced as

$$\Sigma(\mathbf{k}s, E) \approx \frac{K_0}{4\pi(1 - \alpha)^2} \left\{ (E - \tilde{\Sigma}) \left[\ln \frac{(E - \tilde{\Sigma})^2}{(E - \tilde{\Sigma})^2 - \Lambda^2} + \Lambda^2 \tilde{\xi}^2 \right] - s(1 - \alpha)\hbar v_f k \left[\Lambda^2 - (E - \tilde{\Sigma})^2 \ln \frac{(E - \tilde{\Sigma})^2}{(E - \tilde{\Sigma})^2 - \Lambda^2} \right] \tilde{\xi}^2 \right\}. \tag{E3}$$

Then, for $|E| \ll \Gamma_0$, Eq. (E3) can be further reduced as

$$\Sigma(\mathbf{k}s, E) \approx \frac{K_0}{4\pi(1 - \alpha)^2} \left\{ (E - \Sigma_1) \ln \frac{\Sigma_2^2}{\Lambda^2} + 2(E - \Sigma_1) - i\Sigma_2 \ln \frac{\Sigma_2^2}{\Lambda^2} - s(1 - \alpha)\hbar v_f k \Lambda^2 \tilde{\xi}^2 \right\}. \tag{E4}$$

The above self-consistent equation can be separated into three parts corresponding to the Σ_1 , $i\Sigma_2$, and $-s\alpha\hbar v_f k$ parts in the self-energy function,

$$\begin{aligned}
\Sigma_1 &\approx \frac{K_0}{4\pi(1 - \alpha)^2} \left[(E - \Sigma_1) \ln \frac{\Sigma_2^2}{\Lambda^2} + 2(E - \Sigma_1) \right], & i\Sigma_2 &\approx \frac{K_0}{4\pi(1 - \alpha)^2} (-i\Sigma_2) \ln \frac{\Sigma_2^2}{\Lambda^2}, \\
-s\alpha\hbar v_f k &\approx \frac{K_0}{4\pi(1 - \alpha)^2} [-s(1 - \alpha)\hbar v_f k] \Lambda^2 \tilde{\xi}^2.
\end{aligned} \tag{E5}$$

Solving the above self-consistent equations, we can approximately obtain

$$\Sigma_1 \approx -\frac{2\pi(1 - \alpha)^2}{K_0} E, \quad \Sigma_2 \approx -\Lambda e^{-\frac{2\pi(1 - \alpha)^2}{K_0}}, \quad \alpha \approx \frac{1}{2} - \sqrt{\frac{1}{4} - K_0 \frac{\xi^2 k_c^2}{8\pi}}. \tag{E6}$$

For $|E| \gg \Gamma_0$, Eq. (E3) can be further reduced as

$$\Sigma(\mathbf{k}s, E) \approx \frac{K_0}{4\pi(1 - \alpha)^2} \left\{ E \ln \frac{E^2}{\Lambda^2} - i\pi|E| + (E - i\Sigma_2)\Lambda^2 \tilde{\xi}^2 - s(1 - \alpha)\hbar v_f k \Lambda^2 \tilde{\xi}^2 \right\}. \tag{E7}$$

Similarly, this self-consistent equation can be solved by separating into three parts:

$$\begin{aligned}\Sigma_1 &\approx \frac{K_0}{4\pi(1-\alpha)^2} \left(E \ln \frac{E^2}{\Lambda^2} + E \Lambda^2 \xi^2 \right), & i\Sigma_2 &\approx \frac{K_0}{4\pi(1-\alpha)^2} (-i\pi|E| - i\Sigma_2 \Lambda^2 \xi^2), \\ s\alpha \hbar v_f k &\approx \frac{K_0}{4\pi(1-\alpha)^2} [-s(1-\alpha) \hbar v_f k] \Lambda^2 \xi^2.\end{aligned}\quad (\text{E8})$$

Solving the above self-consistent equations, we can approximately obtain

$$\Sigma_1 \approx \frac{K_0}{4\pi(1-\alpha)^2} E \ln \frac{E^2}{\Lambda^2} + \frac{K_0 \xi^2 k_c^2}{8\pi(1-\alpha)^2} E, \quad \Sigma_2 \approx -\frac{\pi K_0}{4\pi(1-\alpha)^2} |E|, \quad \alpha \approx \frac{1}{2} - \sqrt{\frac{1}{4} - K_0 \frac{\xi^2 k_c^2}{8\pi}}. \quad (\text{E9})$$

Combining Eq. (E6) and Eq. (E9), the resulting self-energy function obtained from SCBA is

$$\Sigma(\mathbf{k}s, E) \approx \begin{cases} -\frac{2\pi(1-\alpha)^2}{K_0} E - s\alpha \hbar v_f k - i\Lambda e^{-\frac{2\pi(1-\alpha)^2}{K_0}}, & |E| \ll \Gamma_0, \\ \frac{K_0}{4\pi(1-\alpha)^2} E \ln \frac{E^2}{\Lambda^2} + \frac{\alpha}{1-\alpha} E - s\alpha \hbar v_f k - i\frac{\pi K_0}{4\pi(1-\alpha)^2} |E|, & |E| \gg \Gamma_0, \end{cases} \quad (\text{E10})$$

with

$$\alpha = \frac{1}{2} - \sqrt{\frac{1}{4} - K_0 \frac{\xi^2 k_c^2}{8\pi}}. \quad (\text{E11})$$

2. $\xi \gg a$

At this limit, Eq. (E2) is reduced as

$$\Sigma(\mathbf{k}s, E) \approx \frac{K_0}{4\pi(1-\alpha)^2} \{ (E - \tilde{\Sigma}) \text{Ei}[(E - \tilde{\Sigma})^2 \xi^2] - s(1-\alpha) \hbar v_f k + s(1-\alpha) \hbar v_f k (E - \tilde{\Sigma})^2 \xi^2 \text{Ei}[(E - \tilde{\Sigma})^2 \xi^2] \}. \quad (\text{E12})$$

Then, for $|E| \ll \Gamma_0$, Eq. (E12) can be further reduced as

$$\Sigma_1 + i\Sigma_2 - s\alpha \hbar v_f k \approx \frac{K_0}{4\pi(1-\alpha)^2} \{ (E - \Sigma_1)(2 + \gamma + 2 \ln |\Sigma_2 \xi|) - i\Sigma_2(\gamma + 2 \ln |\Sigma_2 \xi|) - s(1-\alpha) \hbar v_f k \}. \quad (\text{E13})$$

The above self-consistent equation can be separated into three parts corresponding to the Σ_1 , $i\Sigma_2$, and $-s\alpha \hbar v_f k$ parts in the self-energy function,

$$\begin{aligned}\Sigma_1 &\approx \frac{K_0}{4\pi(1-\alpha)^2} [(E - \Sigma_1)(\gamma + 2 \ln |\Sigma_2 \xi|) + 2(E - \Sigma_1)], & i\Sigma_2 &\approx \frac{K_0}{4\pi(1-\alpha)^2} (-i\Sigma_2)(\gamma + 2 \ln |\Sigma_2 \xi|), \\ -s\alpha \hbar v_f k &\approx \frac{K_0}{4\pi(1-\alpha)^2} [-s(1-\alpha) \hbar v_f k].\end{aligned}\quad (\text{E14})$$

Solving the above self-consistent equations, we can approximately obtain

$$\Sigma_1 \approx -\frac{2\pi(1-\alpha)^2}{K_0} E, \quad \Sigma_2 \approx -\frac{\sqrt{2}(1-\alpha) \hbar v_f}{\xi} e^{-\frac{2\pi(1-\alpha)^2}{K_0}}, \quad \alpha \approx \frac{1}{2} - \sqrt{\frac{1}{4} - \frac{K_0}{4\pi}}. \quad (\text{E15})$$

On the other hand, for $|E| \gg \Gamma_0$, Eq. (E12) can be further reduced as

$$\Sigma_1 + i\Sigma_2 - s\alpha \hbar v_f k \approx \frac{K_0}{4\pi(1-\alpha)^2} \{ E(\gamma + 2 \ln |E \xi|) - i\pi|E| - i(2 + \gamma + 2 \ln |E \xi|) \Sigma_2 - s(1-\alpha) \hbar v_f k \}. \quad (\text{E16})$$

Similarly, this self-consistent equation can be solved by separating into three parts:

$$\begin{aligned}\Sigma_1 &\approx \frac{K_0}{4\pi(1-\alpha)^2} E(\gamma + 2 \ln |E \xi|), & i\Sigma_2 &\approx \frac{K_0}{4\pi(1-\alpha)^2} [-i\pi|E| - i\Sigma_2(2 + \gamma + 2 \ln |E \xi|)], \\ s\alpha \hbar v_f k &\approx \frac{K_0}{4\pi(1-\alpha)^2} [-s(1-\alpha) \hbar v_f k].\end{aligned}\quad (\text{E17})$$

Solving the above self-consistent equations, we can approximately obtain

$$\Sigma_1 \approx \frac{K_0}{4\pi(1-\alpha)^2} E(\gamma + 2 \ln |E \xi|), \quad \Sigma_2 \approx -\frac{\pi K_0}{4\pi(1-\alpha)^2} |E|, \quad \alpha \approx \frac{1}{2} - \sqrt{\frac{1}{4} - \frac{K_0}{4\pi}}. \quad (\text{E18})$$

Combining Eq. (E15) and Eq. (E18), the resulting self-energy function obtained from SCBA is

$$\Sigma(\mathbf{k}s, E) \approx \begin{cases} -\frac{2\pi(1-\alpha)^2}{K_0}E - s\alpha\hbar v_f k - i\frac{\sqrt{2}(1-\alpha)\hbar v_f}{\xi}e^{-\frac{2\pi(1-\alpha)^2}{K_0}}, & |E| \ll \Gamma_0, \\ \frac{K_0}{4\pi(1-\alpha)^2}E(\gamma + 2 \ln |E\xi|) + \frac{\alpha}{1-\alpha}E - s\alpha\hbar v_f k - i\frac{\pi K_0}{4\pi(1-\alpha)^2}|E|, & |E| \gg \Gamma_0, \end{cases} \quad (\text{E19})$$

with

$$\alpha = \frac{1}{2} - \sqrt{\frac{1}{4} - \frac{K_0}{4\pi}}. \quad (\text{E20})$$

APPENDIX F: WILSON'S RENORMALIZATION GROUP

In the following, we perform a Wilson's renormalization group calculation in the presence of the long-ranged Gaussian potential.

a. Generating functional. At first, we expand the generating functional with cutoff prescription and disorder averaging. For simplicity, we set sources $\bar{\eta} = 0$ and $\eta = 0$:

$$\begin{aligned} \langle Z \rangle &= \left\langle \int D[\bar{\Psi}, \Psi]_{\Lambda} \exp \left[i \int dt d^2\mathbf{x} \bar{\Psi}_{x,t} (i\partial_t + iv_f \nabla \cdot \boldsymbol{\sigma}) \Psi_{x,t} \right] \exp \left[-i \int dt d^2\mathbf{x} V(\mathbf{x}) \bar{\Psi}_{x,t} \Psi_{x,t} \right] \right\rangle \\ &= \int D[\bar{\Psi}, \Psi]_{\Lambda} \exp \left[\int \frac{d\omega}{2\pi} \frac{d^2\mathbf{k}}{(2\pi)^2} \bar{\Psi}_{k\omega} (i\omega - v_f \mathbf{k} \cdot \boldsymbol{\sigma}) \Psi_{k\omega} \right] \left[1 + \frac{1}{2} \int d\tau d\tau' \frac{d^2\mathbf{q} d^2\mathbf{k} d^2\mathbf{k}'}{(2\pi)^6} \mathcal{K}(\mathbf{q}) \bar{\Psi}_{k,\tau} \Psi_{k-q,\tau} \bar{\Psi}_{k',\tau'} \Psi_{k'+q,\tau'} \right. \\ &\quad + \frac{1}{8} \int d\tau_1 d\tau_2 d\tau_3 d\tau_4 \frac{d^2\mathbf{q} d^2\mathbf{k}_1 d^2\mathbf{k}_2 d^2\mathbf{q}' d^2\mathbf{k}_3 d^2\mathbf{k}_4}{(2\pi)^6} \mathcal{K}(\mathbf{q}) \mathcal{K}(\mathbf{q}') \bar{\Psi}_{k_1,\tau_1} \Psi_{k_1-q,\tau_1} \bar{\Psi}_{k_2,\tau_2} \Psi_{k_2+q,\tau_2} \bar{\Psi}_{k_3,\tau_3} \Psi_{k_3-q',\tau_3} \bar{\Psi}_{k_4,\tau_4} \Psi_{k_4+q',\tau_4} \\ &\quad \left. + \dots \right] \end{aligned} \quad (\text{F1})$$

Notice that there are three combinations of $\langle V(\mathbf{x}_1)V(\mathbf{x}_2) \rangle \langle V(\mathbf{x}_3)V(\mathbf{x}_4) \rangle$. Here, we have transformed real time into imaginary time through Wick's rotation, $it \rightarrow \tau$, since it is convenient to use Matsubara Green's functions in the following calculations.

b. Momentum shell decomposition. According to Wilson's approach, we divide the field operators $\bar{\Psi}(\mathbf{k})$ and $\Psi(\mathbf{k})$ into two groups by a dimensionless variable $b > 1$,

$$\bar{\Psi}(\mathbf{k}) = \begin{cases} \bar{\Psi}^<(\mathbf{k}), & 0 \leq |\mathbf{k}| < \Lambda/b, \\ \bar{\Psi}^>(\mathbf{k}), & \Lambda/b \leq |\mathbf{k}| < \Lambda, \end{cases} \quad \Psi(\mathbf{k}) = \begin{cases} \Psi^<(\mathbf{k}), & 0 \leq |\mathbf{k}| < \Lambda/b, \\ \Psi^>(\mathbf{k}), & \Lambda/b \leq |\mathbf{k}| < \Lambda. \end{cases} \quad (\text{F2})$$

We replace the old $\bar{\Psi}$ and Ψ with $\bar{\Psi}^< + \bar{\Psi}^>$ and $\Psi^< + \Psi^>$ and rewrite the generating functional as

$$\begin{aligned} \langle Z \rangle &= \int D[\bar{\Psi}^<, \Psi^<] e^{S_0[\bar{\Psi}^<, \Psi^<]} \left\{ \int D[\bar{\Psi}^>, \Psi^>] e^{S_0[\bar{\Psi}^>, \Psi^>]} \right\} \left\{ 1 + \frac{1}{2} \int d\tau d\tau' \frac{d^2\mathbf{q} d^2\mathbf{k} d^2\mathbf{k}'}{(2\pi)^6} \mathcal{K}(\mathbf{q}) \bar{\Psi}_{k,\tau}^< \Psi_{k-q,\tau}^< \Psi_{k'+q,\tau'}^< \bar{\Psi}_{k',\tau'}^< \right. \\ &\quad - \int d\tau d\tau' \frac{d^2\mathbf{k}}{(2\pi)^2} \bar{\Psi}_{k,\tau}^< \Psi_{k,\tau'}^< \int \frac{d^2\mathbf{p}}{(2\pi)^2} \mathcal{K}(\mathbf{k} - \mathbf{p}) \mathcal{G}^{>,0}(\mathbf{p}, \tau - \tau') \\ &\quad + \frac{1}{2} \int d\tau_1 d\tau_2 d\tau_3 d\tau_4 \frac{d^2\mathbf{q} d^2\mathbf{k} d^2\mathbf{k}'}{(2\pi)^6} \bar{\Psi}_{k,\tau_1}^< \Psi_{k-q,\tau_3}^< \bar{\Psi}_{k',\tau_4}^< \Psi_{k'+q,\tau_2}^< \int \frac{d^2\mathbf{p}}{(2\pi)^2} \mathcal{K}(\mathbf{k} - \mathbf{p}) \mathcal{K}(\mathbf{p} + \mathbf{q} - \mathbf{k}) \mathcal{G}_{p,\tau_1-\tau_3}^{>,0} \mathcal{G}_{k'+q-k+p,\tau_4-\tau_2}^{>,0} \\ &\quad + \frac{1}{2} \int d\tau_1 d\tau_2 d\tau_3 d\tau_4 \frac{d^2\mathbf{q} d^2\mathbf{k} d^2\mathbf{k}'}{(2\pi)^6} \bar{\Psi}_{k,\tau_1}^< \Psi_{k-q,\tau_4}^< \bar{\Psi}_{k',\tau_2}^< \Psi_{k'+q,\tau_3}^< \int \frac{d^2\mathbf{p}}{(2\pi)^2} \mathcal{K}(\mathbf{k} - \mathbf{p}) \mathcal{K}(\mathbf{p} - \mathbf{k} + \mathbf{q}) \mathcal{G}_{p,\tau_1-\tau_4}^{>,0} \mathcal{G}_{k+k'-p,\tau_2-\tau_3}^{>,0} \\ &\quad \left. + \int d\tau_1 d\tau_2 d\tau_3 d\tau_4 \frac{d^2\mathbf{q} d^2\mathbf{k} d^2\mathbf{k}'}{(2\pi)^6} \bar{\Psi}_{k,\tau_1}^< \Psi_{k-q,\tau_1}^< \bar{\Psi}_{k',\tau_4}^< \Psi_{k'+q,\tau_3}^< \int \frac{d^2\mathbf{p}}{(2\pi)^2} \mathcal{K}(\mathbf{q}) \mathcal{K}(\mathbf{k}' - \mathbf{p}) \mathcal{G}_{p,\tau_2-\tau_3}^{>,0} \mathcal{G}_{p+q,\tau_4-\tau_2}^{>,0} + \dots \right\}, \quad (\text{F3}) \end{aligned}$$

where $S_0[\bar{\Psi}^<, \Psi^<] = \int \frac{d\omega}{2\pi} \frac{d^2\mathbf{k}}{(2\pi)^2} \bar{\Psi}_{k,\omega}^< (i\omega - v_f \mathbf{k} \cdot \boldsymbol{\sigma}) \Psi_{k,\omega}^<$ is the unperturbed action in the momentum shell $|\mathbf{k}| < \Lambda/b$, $S_0[\bar{\Psi}^>, \Psi^>] = \int \frac{d\omega}{2\pi} \frac{d^2\mathbf{k}}{(2\pi)^2} \bar{\Psi}_{k,\omega}^> (i\omega - v_f \mathbf{k} \cdot \boldsymbol{\sigma}) \Psi_{k,\omega}^>$ is the unperturbed action in the momentum shell $\Lambda/b < |\mathbf{k}| < \Lambda$, and $\langle \bar{\Psi}_1^> \Psi_2^> \rangle = \frac{\int D[\bar{\Psi}^>, \Psi^>] \bar{\Psi}_1^> \Psi_2^> e^{S_0[\bar{\Psi}^>, \Psi^>]}}{\int D[\bar{\Psi}^>, \Psi^>] e^{S_0[\bar{\Psi}^>, \Psi^>]}} = -\mathcal{G}_{12}^{>,0}$ denotes the unperturbed correction function for the fields $\bar{\Psi}^>$ and $\Psi^>$. The four terms containing the integral of $\mathcal{G}^{>,0}$ in the brace correspond in turn to the four one-loop RG diagrams shown in Fig. 2. The diagram (a) is responsible for the renormalization of the energy and velocity, while others are for disorder coupling. Additionally, diagram (a) has two degenerates due to the exchange $\tau \leftrightarrow \tau'$. Diagrams (b) and (c) have four degenerates due to the exchanges $\tau_1 \leftrightarrow \tau_2$ and $(\tau_1, \tau_2) \leftrightarrow (\tau_3, \tau_4)$. Diagram (d) has eight degenerates due to the exchanges $\tau_1 \leftrightarrow \tau_2$, $\tau_3 \leftrightarrow \tau_4$, and $(\tau_1, \tau_2) \leftrightarrow (\tau_3, \tau_4)$.

c. Corrections of the energy, momentum, and disorder coupling. According to Eq. (F3), we can get the corrections of the energy, momentum, and disorder coupling after performing the integral over $\Psi^>$ ($\Psi^>$). The corresponding four RG diagrams in Fig. 2 are calculated one by one. When calculating the diagrams of the renormalization of disorder coupling, we assume that the momenta of the external lines are zero:

$$\begin{aligned}
I^{(a)} &= - \int_{[\Lambda/b, \Lambda]} \frac{d^2 \mathbf{p}}{(2\pi)^2} \mathcal{K}(\mathbf{k} - \mathbf{p}) \mathcal{G}^0(\mathbf{p}, \omega) \\
&= -K_0 (\hbar v_f)^2 \int_{[\Lambda/b, \Lambda]} \frac{d^2 \mathbf{p}}{(2\pi)^2} e^{-\frac{\xi^2 |\mathbf{k}-\mathbf{p}|^2}{2}} \frac{1}{i\omega - \hbar v_f \mathbf{p} \cdot \boldsymbol{\sigma}} = -K_0 (\hbar v_f)^2 \int_{[\Lambda/b, \Lambda]} \frac{d^2 \mathbf{p}}{(2\pi)^2} e^{-\frac{\xi^2 |\mathbf{k}-\mathbf{p}|^2}{2}} \frac{i\omega + \hbar v_f \mathbf{p} \cdot \boldsymbol{\sigma}}{\omega^2 + (\hbar v_f p)^2} \\
&= \frac{K_0 (\hbar v_f)^2}{4\pi^2} \int_{-\pi}^{\pi} d\theta \int_{\Lambda/b}^{\Lambda} p dp e^{-\frac{\xi^2 (k^2 + p^2 - 2kp \cos \theta)}{2}} \left[\frac{i\omega}{\omega^2 + (\hbar v_f p)^2} + \frac{\hbar v_f p \cos \theta}{\omega^2 + (\hbar v_f p)^2} \frac{\mathbf{k} \cdot \boldsymbol{\sigma}}{k} \right] \\
&\approx \frac{K_0}{4\pi^2} \int_{-\pi}^{\pi} d\theta \int_{\Lambda/b}^{\Lambda} dp e^{-\frac{\xi^2 (k^2 + p^2 - 2kp \cos \theta)}{2}} \left[\frac{i\omega}{p} + \cos \theta \frac{\hbar v_f \mathbf{k} \cdot \boldsymbol{\sigma}}{k} \right] \\
&= \frac{K_0}{2\pi} \int_{\Lambda/b}^{\Lambda} dp e^{-\frac{\xi^2 (k^2 + p^2)}{2}} \left[I_0(kp\xi^2) \frac{i\omega}{p} + I_1(kp\xi^2) \frac{\hbar v_f \mathbf{k} \cdot \boldsymbol{\sigma}}{k} \right] \\
&\approx \left[\left(1 - \frac{1}{b}\right) \frac{K_0}{2\pi} e^{-\frac{\xi^2 \Lambda^2}{2}} \right] i\omega + \left[\left(1 - \frac{1}{b}\right) \frac{K_0 \xi^2 \Lambda^2}{4\pi} e^{-\frac{\xi^2 \Lambda^2}{2}} \right] \hbar v_f \mathbf{k} \cdot \boldsymbol{\sigma}. \tag{F4}
\end{aligned}$$

Here, we have assumed $k\xi \ll 1$, and the modified Bessel functions are expanded as $I_0(x) = 1 + \frac{x^2}{4} + o(x^3)$ and $I_1(x) = \frac{x}{2} + o(x^3)$. Meanwhile, θ is the angle between the momenta \mathbf{k} and \mathbf{p} . The $\mathbf{p} \cdot \boldsymbol{\sigma}$ in the above derivation is transformed by

$$\begin{aligned}
\mathbf{p} \cdot \boldsymbol{\sigma} &= p \cos \theta_p \sigma_x + p \sin \theta_p \sigma_y = p \cos(\theta_k + \theta) \sigma_x + p \sin(\theta_k + \theta) \sigma_y \\
&\rightarrow \frac{p}{k} [k \cos \theta_k \cos \theta \sigma_x + k \sin \theta_k \cos \theta \sigma_y] \\
&= \frac{p}{k} \cos \theta \mathbf{k} \cdot \boldsymbol{\sigma}, \tag{F5}
\end{aligned}$$

where the terms proportional to $\sin \theta$ are omitted based on the parity analysis of the integral:

$$\begin{aligned}
I^{(b)} &= \int_{[\Lambda/b, \Lambda]} \frac{d^2 \mathbf{p}}{(2\pi)^2} \mathcal{K}(-\mathbf{p}) \mathcal{K}(\mathbf{p}) \mathcal{G}^0(\mathbf{p}, \omega) \mathcal{G}^0(\mathbf{p}, \omega) = K_0^2 (\hbar v_f)^4 \int_{[\Lambda/b, \Lambda]} \frac{d^2 \mathbf{p}}{(2\pi)^2} e^{-\xi^2 p^2} \frac{1}{i\omega - \hbar v_f \mathbf{p} \cdot \boldsymbol{\sigma}} \frac{1}{i\omega - \hbar v_f \mathbf{p} \cdot \boldsymbol{\sigma}} \\
&= K_0^2 (\hbar v_f)^4 \int_{[\Lambda/b, \Lambda]} \frac{d^2 \mathbf{p}}{(2\pi)^2} e^{-\xi^2 p^2} \frac{(i\omega + \hbar v_f \mathbf{p} \cdot \boldsymbol{\sigma})^2}{[\omega^2 + (\hbar v_f p)^2]^2} \approx \left(1 - \frac{1}{b}\right) \frac{K_0^2 (\hbar v_f)^2}{2\pi} e^{-\xi^2 \Lambda^2}, \tag{F6}
\end{aligned}$$

$$\begin{aligned}
I^{(c)} &= \int_{[\Lambda/b, \Lambda]} \frac{d^2 \mathbf{p}}{(2\pi)^2} \mathcal{K}(-\mathbf{p}) \mathcal{K}(\mathbf{p}) \mathcal{G}^0(\mathbf{p}, \omega) \mathcal{G}^0(-\mathbf{p}, \omega) = K_0^2 (\hbar v_f)^4 \int_{[\Lambda/b, \Lambda]} \frac{d^2 \mathbf{p}}{(2\pi)^2} e^{-\xi^2 p^2} \frac{1}{i\omega - \hbar v_f \mathbf{p} \cdot \boldsymbol{\sigma}} \frac{1}{i\omega + \hbar v_f \mathbf{p} \cdot \boldsymbol{\sigma}} \\
&= K_0^2 (\hbar v_f)^4 \int_{[\Lambda/b, \Lambda]} \frac{d^2 \mathbf{p}}{(2\pi)^2} e^{-\xi^2 p^2} \frac{(i\omega + \hbar v_f \mathbf{p} \cdot \boldsymbol{\sigma})(i\omega - \hbar v_f \mathbf{p} \cdot \boldsymbol{\sigma})}{[\omega^2 + (\hbar v_f p)^2]^2} \approx -\left(1 - \frac{1}{b}\right) \frac{K_0^2 (\hbar v_f)^2}{2\pi} e^{-\xi^2 \Lambda^2}, \tag{F7}
\end{aligned}$$

$$\begin{aligned}
I^{(d)} &= \int_{[\Lambda/b, \Lambda]} \frac{d^2 \mathbf{p}}{(2\pi)^2} \mathcal{K}(0) \mathcal{K}(-\mathbf{p}) \mathcal{G}^0(\mathbf{p}, \omega) \mathcal{G}^0(\mathbf{p}, \omega) = K_0^2 (\hbar v_f)^4 \int_{[\Lambda/b, \Lambda]} \frac{d^2 \mathbf{p}}{(2\pi)^2} e^{-\xi^2 p^2/2} \frac{1}{i\omega - \hbar v_f \mathbf{p} \cdot \boldsymbol{\sigma}} \frac{1}{i\omega - \hbar v_f \mathbf{p} \cdot \boldsymbol{\sigma}} \\
&= K_0^2 (\hbar v_f)^4 \int_{[\Lambda/b, \Lambda]} \frac{d^2 \mathbf{p}}{(2\pi)^2} e^{-\xi^2 p^2/2} \frac{(i\omega + \hbar v_f \mathbf{p} \cdot \boldsymbol{\sigma})^2}{[\omega^2 + (\hbar v_f p)^2]^2} \approx \left(1 - \frac{1}{b}\right) \frac{K_0^2 (\hbar v_f)^2}{2\pi} e^{-\frac{\xi^2 \Lambda^2}{2}}, \tag{F8}
\end{aligned}$$

where the results of RG diagrams (b) [$I^{(b)}$] and (c) [$I^{(c)}$] cancel each other out.

Plugging Eqs. (F4)–(F8) into Eq. (F3), therefore, we can get the effective generating functional in the shell $|k| < \Lambda/b$ as

$$\begin{aligned}
\langle Z \rangle_{\text{eff}} &= \int D[\bar{\Psi}^<, \Psi^<] e^{S_0[\bar{\Psi}^<, \Psi^<]} \left\{ 1 + \frac{1}{2} \int d\tau d\tau' \frac{d^2 \mathbf{q} d^2 \mathbf{k} d^2 \mathbf{k}'}{(2\pi)^6} \mathcal{K}(\mathbf{q}) \bar{\Psi}_{\mathbf{k}, \tau}^< \Psi_{\mathbf{k}-\mathbf{q}, \tau}^< \Psi_{\mathbf{k}'+\mathbf{q}, \tau'}^< \bar{\Psi}_{\mathbf{k}', \tau'}^< \right. \\
&\quad \left. + \int \frac{d\omega}{2\pi} \frac{d^2 \mathbf{k}}{(2\pi)^2} \bar{\Psi}_{\mathbf{k}, \omega}^< \Psi_{\mathbf{k}, \omega}^< (\Delta_E i\omega + \alpha \hbar v_f \mathbf{k} \cdot \boldsymbol{\sigma}) + \Delta_K \int d\tau_1 d\tau_2 \frac{d^2 \mathbf{q} d^2 \mathbf{k} d^2 \mathbf{k}'}{(2\pi)^6} \bar{\Psi}_{\mathbf{k}, \tau_1}^< \Psi_{\mathbf{k}-\mathbf{q}, \tau_1}^< \bar{\Psi}_{\mathbf{k}', \tau_2}^< \Psi_{\mathbf{k}'+\mathbf{q}, \tau_2}^< \right\}
\end{aligned}$$

$$\begin{aligned} &\approx \int D[\bar{\Psi}, \Psi]_{\Lambda/b} \exp \left\{ \int \frac{d\omega}{2\pi} \frac{d^2\mathbf{k}}{(2\pi)^2} \bar{\Psi}_{\mathbf{k},\omega} [(1 + \Delta_E)i\omega - (1 - \alpha)\hbar v_f \mathbf{k} \cdot \boldsymbol{\sigma}] \Psi_{\mathbf{k},\omega} \right. \\ &\quad \left. + \frac{1}{2} \int d\tau d\tau' \frac{d^2\mathbf{q} d^2\mathbf{k} d^2\mathbf{k}'}{(2\pi)^6} [\mathcal{K}(\mathbf{q}) + 2\Delta_K] \bar{\Psi}_{\mathbf{k},\tau} \Psi_{\mathbf{k}-\mathbf{q},\tau} \Psi_{\mathbf{k}'+\mathbf{q},\tau'} \bar{\Psi}_{\mathbf{k}',\tau'} \right\}, \end{aligned} \quad (\text{F9})$$

with

$$\Delta_E = \left(1 - \frac{1}{b}\right) \frac{K_0}{2\pi} e^{-\frac{\xi^2 \Lambda^2}{2}}, \quad \alpha = \left(1 - \frac{1}{b}\right) \frac{K_0 \xi^2 \Lambda^2}{4\pi} e^{-\frac{\xi^2 \Lambda^2}{2}}, \quad \Delta_K = \left(1 - \frac{1}{b}\right) \frac{K_0^2 (\hbar v_f)^2}{2\pi} e^{-\frac{\xi^2 \Lambda^2}{2}}. \quad (\text{F10})$$

The coefficient $\{\int D[\bar{\Psi}^>, \Psi^>] e^{S_0[\bar{\Psi}^>, \Psi^>]}\}$ is eliminated since it will be absorbed into the normalization of the generating function.

d. Renormalization group flow. Let us now rescale momenta and fields in the effective generating functional according to

$$\mathbf{k}' = b\mathbf{k}, \quad \bar{\Psi}'(\Psi') = b^{-3/2} \bar{\Psi}(\Psi), \quad (\text{F11})$$

so that the momentum \mathbf{k}' is integrated over $|\mathbf{k}'| < \Lambda$. The rescaling of fields is to keep the free propagator unchanged. The rescaled effective generating functional is

$$\begin{aligned} \langle Z \rangle_{\text{eff}} &= \int D[\bar{\Psi}', \Psi']_{\Lambda} \exp \left\{ \int \frac{d\omega}{2\pi} \frac{d^2\mathbf{k}'}{(2\pi)^2} \bar{\Psi}'_{\mathbf{k}',\omega} [b(1 + \Delta_E)i\omega - (1 - \alpha)\hbar v_f \mathbf{k}' \cdot \boldsymbol{\sigma}] \Psi'_{\mathbf{k}',\omega} \right. \\ &\quad \left. + \frac{1}{2} \int d\tau d\tau' \frac{d^2\mathbf{q} d^2\mathbf{k} d^2\mathbf{k}'}{(2\pi)^6} [\mathcal{K}(\mathbf{q}) + 2\Delta_K] \bar{\Psi}'_{\mathbf{k},\tau} \Psi'_{\mathbf{k}-\mathbf{q},\tau} \Psi'_{\mathbf{k}'+\mathbf{q},\tau'} \bar{\Psi}'_{\mathbf{k}',\tau'} \right\}, \end{aligned} \quad (\text{F12})$$

which gives the transformation laws of energy, velocity, and disorder,

$$\begin{aligned} E' &= b(1 + \Delta_E)E = b \left[1 + \left(1 - \frac{1}{b}\right) \frac{K_0}{2\pi} e^{-\frac{\xi^2 \Lambda^2}{2}} \right] E, \quad v'_f = (1 - \alpha)v_f = \left[1 - \left(1 - \frac{1}{b}\right) \frac{K_0 \xi^2 \Lambda^2}{4\pi} e^{-\frac{\xi^2 \Lambda^2}{2}} \right] v_f, \\ K'_0 &= K_0 + \left(1 - \frac{1}{b}\right) \frac{K_0^2}{\pi} e^{-\frac{\xi^2 \Lambda^2}{2}}, \end{aligned} \quad (\text{F13})$$

where we only consider the leading term of disorder coupling $\mathcal{K}(\mathbf{q}) \rightarrow K_0(\hbar v_f)^2$ and do the analytic continuation for energy, $i\omega \rightarrow E + i0^+$.

Then we replace the renormalization parameter by $b = e^{dl} \approx 1 + dl$, where dl is the running ultraviolet cutoff length. Thus the one-loop renormalization group equations of the running energy \tilde{E} , velocity \tilde{v}_f , and disorder coupling \tilde{K}_0 are given by

$$\frac{d\tilde{E}}{dl} = \left(1 + \frac{\tilde{K}_0}{2\pi} e^{-\frac{\Lambda^2 \xi^2}{2}}\right) \tilde{E}, \quad \frac{d\tilde{v}_f}{dl} = -\frac{\tilde{K}_0 \xi^2 \Lambda^2}{4\pi} e^{-\frac{\xi^2 \Lambda^2}{2}} \tilde{v}_f, \quad \frac{d\tilde{K}_0}{dl} = \frac{\tilde{K}_0^2}{\pi} e^{-\frac{\Lambda^2 \xi^2}{2}}. \quad (\text{F14})$$

We can also express the result in the form of momentum space running with $dl = -d \ln \Lambda$. This amounts to changing the sign of the derivations and the RG equations are rewritten as

$$\frac{d\tilde{E}}{d \ln \Lambda} = -\left(1 + \frac{\tilde{K}_0}{2\pi} e^{-\frac{\Lambda^2 \xi^2}{2}}\right) \tilde{E}, \quad \frac{d\tilde{v}_f}{d \ln \Lambda} = \frac{\tilde{K}_0 \xi^2 \Lambda^2}{4\pi} e^{-\frac{\xi^2 \Lambda^2}{2}} \tilde{v}_f, \quad \frac{d\tilde{K}_0}{d \ln \Lambda} = -\frac{\tilde{K}_0^2}{\pi} e^{-\frac{\Lambda^2 \xi^2}{2}}. \quad (\text{F15})$$

-
- [1] K. S. Novoselov, A. K. Geim, S. V. Morozov, D. Jiang, M. I. Katsnelson, I. V. Grigorieva, S. V. Dubonos, and A. A. Firsov, Two-dimensional gas of massless Dirac fermions in graphene, *Nature (London)* **438**, 197 (2005).
- [2] K. S. Novoselov, D. Jiang, F. Schedin, T. J. Booth, V. V. Khotkevich, S. V. Morozov, and A. K. Geim, Two-dimensional atomic crystals, *Proc. Natl. Acad. Sci. USA* **102**, 10451 (2005).
- [3] A. W. W. Ludwig, M. P. Fisher, R. Shankar, and G. Grinstein, Integer quantum Hall transition: An alternative approach and exact results, *Phys. Rev. B* **50**, 7526 (1994).
- [4] N. H. Shon and T. Ando, Quantum transport in two-dimensional graphite system, *J. Phys. Soc. Jpn.* **67**, 2421 (1998).
- [5] P. A. Lee, Localized states in a d -wave superconductor, *Phys. Rev. Lett.* **71**, 1887 (1993).
- [6] A. C. Durst and P. A. Lee, Impurity-induced quasiparticle transport and universal-limit Wiedemann-Franz violation in d -wave superconductors, *Phys. Rev. B* **62**, 1270 (2000).
- [7] S. Das Sarma, S. Adam, E. H. Hwang, and E. Rossi, Electronic transport in two-dimensional graphene, *Rev. Mod. Phys.* **83**, 407 (2011).
- [8] Y. Zhang, Y.-W. Tan, H. L. Stormer, and P. Kim, Experimental observation of the quantum Hall effect and Berry's phase in graphene, *Nature (London)* **438**, 201 (2005).
- [9] Y.-W. Tan, Y. Zhang, K. Bolotin, Y. Zhao, S. Adam, E. H. Hwang, S. Das Sarma, H. L. Stormer, and P. Kim, Measurement of scattering rate and minimum conductivity in graphene, *Phys. Rev. Lett.* **99**, 246803 (2007).

- [10] K. I. Bolotin, K. J. Sikes, J. Hone, H. L. Stormer, and P. Kim, Temperature-dependent transport in suspended graphene, *Phys. Rev. Lett.* **101**, 096802 (2008).
- [11] X. Du, I. Skachko, A. Barker, and E. Y. Andrei, Approaching ballistic transport in suspended graphene, *Nat. Nanotechnol.* **3**, 491 (2008).
- [12] S. V. Morozov, K. S. Novoselov, M. I. Katsnelson, F. Schedin, D. C. Elias, J. A. Jaszczak, and A. K. Geim, Giant intrinsic carrier mobilities in graphene and its bilayer, *Phys. Rev. Lett.* **100**, 016602 (2008).
- [13] C. R. Dean, A. F. Young, I. Meric, C. Lee, L. Wang, S. Sorgenfrei, K. Watanabe, T. Taniguchi, P. Kim, K. L. Shepard, and J. Hone, Boron nitride substrates for high-quality graphene electronics, *Nat. Nanotechnol.* **5**, 722 (2010).
- [14] P. J. Zomer, S. P. Dash, N. Tombros, and B. J. van Wees, A transfer technique for high mobility graphene devices on commercially available hexagonal boron nitride, *Appl. Phys. Lett.* **99**, 232104 (2011).
- [15] A. S. Mayorov, D. C. Elias, I. S. Mukhin, S. V. Morozov, L. A. Ponomarenko, K. S. Novoselov, A. K. Geim, and R. V. Gorbachev, How close can one approach the Dirac point in graphene experimentally, *Nano Lett.* **12**, 4629 (2012).
- [16] N. J. G. Couto, D. Costanzo, S. Engels, D. K. Ki, K. Watanabe, T. Taniguchi, C. Stampfer, F. Guinea, and A. F. Morpurgo, Random strain fluctuations as dominant disorder source for high-quality on-substrate graphene devices, *Phys. Rev. X* **4**, 041019 (2014).
- [17] L. J. Wang, P. Makk, S. Zihlmann, A. Baumgartner, D. I. Indolese, K. Watanabe, T. Taniguchi, and C. Schonenberger, Mobility enhancement in graphene by *in situ* reduction of random strain fluctuations, *Phys. Rev. Lett.* **124**, 157701 (2020).
- [18] N. M. R. Peres, F. Guinea, and A. H. Castro Neto, Electronic properties of disordered two-dimensional carbon, *Phys. Rev. B* **73**, 125411 (2006).
- [19] P. M. Ostrovsky, I. V. Gornyi, and A. D. Mirlin, Electron transport in disordered graphene, *Phys. Rev. B* **74**, 235443 (2006).
- [20] M. I. Katsnelson, Zitterbewegung, chirality, and minimal conductivity in graphene, *Eur. Phys. J. B* **51**, 157 (2006).
- [21] J. Tworzydło, B. Trauzettel, M. Titov, A. Rycerz, and C. W. J. Beenakker, Sub-poissonian shot noise in graphene, *Phys. Rev. Lett.* **96**, 246802 (2006).
- [22] P. M. Ostrovsky, I. V. Gornyi, and A. D. Mirlin, Conductivity of disordered graphene at half filling, *Eur. Phys. J. Spec. Top.* **148**, 63 (2007).
- [23] P. M. Ostrovsky, I. V. Gornyi, and A. D. Mirlin, Quantum criticality and minimal conductivity in graphene with long-range disorder, *Phys. Rev. Lett.* **98**, 256801 (2007).
- [24] A. Schuessler, P. M. Ostrovsky, I. V. Gornyi, and A. D. Mirlin, Analytic theory of ballistic transport in disordered graphene, *Phys. Rev. B* **79**, 075405 (2009).
- [25] J. H. Bardarson, J. Tworzydło, P. W. Brouwer, and C. W. J. Beenakker, One-Parameter Scaling at the Dirac Point in Graphene, *Phys. Rev. Lett.* **99**, 106801 (2007).
- [26] K. Ziegler, Minimal conductivity of graphene: Nonuniversal values from the Kubo formula, *Phys. Rev. B* **75**, 233407 (2007).
- [27] S. Ryu, C. Mudry, A. Furusaki, and A. W. W. Ludwig, Landauer conductance and twisted boundary conditions for Dirac fermions in two space dimensions, *Phys. Rev. B* **75**, 205344 (2007).
- [28] M. Trushin and J. Schliemann, Minimum electrical and thermal conductivity of graphene: A quasiclassical approach, *Phys. Rev. Lett.* **99**, 216602 (2007).
- [29] S. Adam, E. H. Hwang, V. M. Galitski, and S. Das Sarma, A self-consistent theory for graphene transport, *Proc. Natl. Acad. Sci. USA* **104**, 18392 (2007).
- [30] J. W. Klos and I. V. Zozoulenko, Effect of short- and long-range scattering on the conductivity of graphene: Boltzmann approach vs tight-binding calculations, *Phys. Rev. B* **82**, 081414(R) (2010).
- [31] S. Adam, P. W. Brouwer, and S. Das Sarma, Crossover from quantum to Boltzmann transport in graphene, *Phys. Rev. B* **79**, 201404(R) (2009).
- [32] T. M. Radchenko, A. A. Shylau, and I. V. Zozoulenko, Influence of correlated impurities on conductivity of graphene sheets: Time-dependent real-space Kubo approach, *Phys. Rev. B* **86**, 035418 (2012).
- [33] H. Suzuura and T. Ando, Crossover from symplectic to orthogonal class in a two-dimensional Honeycomb lattice, *Phys. Rev. Lett.* **89**, 266603 (2002).
- [34] X.-Z. Yan and C. S. Ting, Weak localization of dirac fermions in graphene, *Phys. Rev. Lett.* **101**, 126801 (2008).
- [35] M. Noro, M. Koshino, and T. Ando, Theory of transport in graphene with long-range scatterers, *J. Phys. Soc. Jpn.* **79**, 094713 (2010).
- [36] K. Nomura and A. H. MacDonald, Quantum transport of massless dirac fermions, *Phys. Rev. Lett.* **98**, 076602 (2007).
- [37] A. Rycerz, J. Tworzydło, and C. W. J. Beenakker, Anomalously large conductance fluctuations in weakly disordered graphene, *Europhys. Lett.* **79**, 57003 (2007).
- [38] L. R. F. Lima and C. H. Lewenkopf, Disorder-assisted transmission due to charge puddles in monolayer graphene: Transmission enhancement and local currents, *Phys. Rev. B* **93**, 045404 (2016).
- [39] Z. Fan, J. H. Garcia, A. W. Cummings, J. E. Barrios-Vargas, M. Panhans, A. Harju, F. Ortmann, and S. Roche, Linear scaling quantum transport methodologies, *Phys. Rep.* **903**, 1 (2021).
- [40] J.-H. Chen, C. Jang, S. Adam, M. S. Fuhrer, E. D. Williams, and M. Ishigami, Charged-impurity scattering in graphene, *Nat. Phys.* **4**, 377 (2008).
- [41] A. A. Fedorenko, D. Carpentier, and E. Orignac, Two-dimensional Dirac fermions in the presence of long-range correlated disorder, *Phys. Rev. B* **85**, 125437 (2012).
- [42] E. Fradkin, Critical behavior of disordered degenerate semiconductors. I. Models, symmetries, and formalism, *Phys. Rev. B* **33**, 3257 (1986); Critical behavior of disordered degenerate semiconductors. II. Spectrum and transport properties in mean-field theory, *ibid.* **33**, 3263 (1986).
- [43] I. L. Aleiner and K. B. Efetov, Effect of disorder on transport in graphene, *Phys. Rev. Lett.* **97**, 236801 (2006).
- [44] A. Altland and M. R. Zirnbauer, Nonstandard symmetry classes in mesoscopic normal-superconducting hybrid structures, *Phys. Rev. B* **55**, 1142 (1997).
- [45] B. Yu-Kuang Hu, E. H. Hwang, and S. Das Sarma, Density of states of disordered graphene, *Phys. Rev. B* **78**, 165411 (2008).

- [46] H. Bruus and C. Flensberg, *Many-Body Quantum Theory in Condensed Matter Physics* (Oxford University Press, New York, 2004).
- [47] I. Gradshteyn and I. Ryzhik, *Table of Integrals, Series, and Products*, 7th ed. (Academic Press, New York, 2007).
- [48] M. Abramowitz and I. A. Stegun, *Handbook of Mathematical Functions With Formulas, Graphs, and Mathematical Tables*, 10th ed. (National Bureau of Standards, Gaithersburg, MD, 1972).
- [49] W. Chen, C. Xiao, Q. Shi, and Q. Li, Spin-orbit related power-law dependence of the diffusive conductivity on the carrier density in disordered Rashba two-dimensional electron systems, [Phys. Rev. B **101**, 020203\(R\) \(2020\)](#).